AGU PUBLICATIONS

JGR

Journal of Geophysical Research: Oceans

RESEARCH ARTICLE

10.1002/2017JC013398

Key Points:

- ^{226}Ra and ^{228}Ra are used to constrain water residence time and submarine groundwater discharge (SGD) in Hainan eastern upwelling (HEU)
- Groundwater borne nutrients and upwelling induced nutrients to the mixing layer are estimated in HEU
- SGD derived nutrient could be significant as a missing dissolved inorganic nitrogen to support the new production in HEU

Supporting Information:

- Supporting Information S1
- Figure S1
- Data Set S1

Correspondence to:
J. J. Jiao,
jjiao@hku.hk

Citation:
Luo, X., Jimmy Jiao, J., Liu, Y., Zhang, X., Liang, W., & Tang, D. (2018). Evaluation of water residence time, submarine groundwater discharge and maximum new production supported by groundwater borne nutrients in a coastal upwelling shelf system. *Journal of Geophysical Research: Oceans*, *123*, 631–655. https://doi.org/10.1002/2017JC013398

Received 28 AUG 2017
Accepted 22 NOV 2017
Accepted article online 8 JAN 2018
Published online 29 JAN 2018

Evaluation of Water Residence Time, Submarine Groundwater Discharge, and Maximum New Production Supported by Groundwater Borne Nutrients in a Coastal Upwelling Shelf System

Xin Luo[1,2], Jiu Jimmy Jiao[1,2], Yi Liu[1,2], Xiaolang Zhang[3], Wenzhao Liang[1], and Danling Tang[4]

[1]Department of Earth Sciences, The University of Hong Kong, China, [2]Shenzhen Research Institute (SRI), The University of Hong Kong, Shenzhen, China, [3]School of Environmental Science and Engineering, South University of Science and Technology of China (SUSTC), Shenzhen, China, [4]State Key Laboratory of Tropical Oceanography, Guangdong Key Laboratory of Ocean Remote Sensing, South China Sea, Institute of Oceanography, Chinese Academy of Sciences, Guangzhou, China

Abstract The biogeochemical processes in the continental shelf systems are usually extensively influenced by coastal upwelling and submarine groundwater discharge (SGD). Using eastern Hainan upwelling shelf system as an example, this study fully investigates SGD and coastal upwelling and their effects on the coastal nutrient loadings to the mixing layer of eastern Hainan shelf. Based on the spatial distributions of ^{223}Ra and ^{228}Ra, water residence time is estimated to be 16.9 ± 8.9 days. Based on the mass balance models of ^{226}Ra and ^{228}Ra, the total SGD of the eastern Hainan shelf is estimated to be 0.8×10^8 and 1.4×10^8 m^3 d^{-1}, respectively. The groundwater borne dissolved inorganic nitrogen (DIN) and dissolved inorganic phosphate (DIP) are estimated to be up to 1121.8 and 20.4 μM m^2 d^{-1}. The coastal upwelling delivers 2741.8 μM m^2 d^{-1} DIN and 217.7 μM m^2 d^{-1} DIP into the mixing layer, which are predominant in all the exogenous nutrient inputs. The groundwater borne DIN will support a maximum new production of 7.5 mM C m^2 d^{-1}, about up to 24.0% of the total new production in the study area. SGD-derived nutrient could be significant as a missing DIN to support the new production in the mixing layer of eastern Hainan shelf. The findings contribute to a better understanding of biogeochemical processes under the influences of SGD and coastal upwelling in the study area and other similar coastal upwelling systems.

1. Introduction

There has been a common recognition of the importance of groundwater borne constitutes to the coasts since 1980s (Johannes & Hearn, 1985; Valiela et al., 1978, 1992). Submarine groundwater discharge (SGD), principally driven by the hydrologic gradient, tidal, and wave pumping, is defined as any or all fluids discharging from the seedbed to the coasts, and considered to be the conveyor delivering significant constitutes to the coasts (Burnett et al., 2003; Moore, 2010; Sawyer et al., 2016).

The SGD occurs in coastal aquifers the scales varying from intertidal, embayment, to continental (Bratton, 2010). The SGD study has been integrated with that of coastal ecosystem dynamics because SGD-borne nutrients are considered to lead to the coastal eutrophication and hypoxia, and maybe be the causative factor of red tide outbreaks (Gonneea & Charette, 2014; Luo & Jiao, 2016; Peterson et al., 2016; Talbot et al., 2003). SGD can occur through the continental shelf due to outcrops or springs of offshore aquifers (Lamontagne et al., 2008, 2015; Swarzenski et al., 2001), advective flow driven by storms, buoyancy, and large tidal fluctuations (Kim et al., 2005; Moore & Wilson, 2005), or the pore water exchanges by other physical driven forces such as flow and topography-induced pressure gradient, fluid shear, density-driven convection, and compaction, etc. (Huettel et al., 1998; Jahnke et al., 2000; Precht & Huettel, 2003; Santos et al., 2012b). Over a continental shelf scale, Kim et al. (2005) established a ^{226}Ra/^{228}Ra model to estimate SGD in the Yellow Sea, and showed that SGD-derived dissolved silica loading constitutes nearly 20–100% ($\approx 23 \times 10^9$ mol yr^{-1}) of total riverine input around the Yellow Sea. Liu et al. (2012) indicated that an amount of 153–347 $\times 10^9$ mol yr^{-1} DIC is delivered to the North South China Sea (NSCS) shelf, which supports nearly 11% new production. With the radium isotopic models, Q. Liu et al. (2014) revealed that the groundwater-borne DIC is the predominant DIC source in the southwest Florida Shelf. Moreover, SGD-derived nutrient loadings can further influence the coastal ecosystem such as inducing the red tide outbreaks, primary productivity (PP), coral reef/system, and seagrass (Blanco et al., 2011; Encarnação et al., 2013; Kotwicki et al., 2014; Luo & Jiao, 2016). Kwon et al. (2014) deployed a ^{228}Ra inverse model which led to a global SGD estimate of $(12 \pm 3) \times 10^{13}$ m^3 yr^{-1}. The global SGD estimate was further refined to be $(4.4 \pm 1.2) \times 10^{13}$ m^3 yr^{-1} by considering geographic and salinity effects on radium activities in groundwater end-member (Cho & Kim, 2016). A modified ^{228}Ra inverse model has been recently developed, which leads to an update global SGD estimate of 1.3 – 14.7 $\times 10^{13}$ m^3 yr^{-1} (Le Gland et al., 2017).

The seawater residence times of the continental shelf can be also quantified via radium isotopic models (Burt et al., 2014; Hancock et al., 2006; Lee et al., 2014, Luo et al., 2014; Moore, 2000). The short-lived radium isotopes are advantageous in quantifying the water mixing rate and residence time over continental shelf scales, as the radium can be primarily sourced from the coast groundwater. Radium isotopes behave relatively conservatively during the transport in the coastal waters. The activity ratios (ARs) of ^{224}Ra/^{223}Ra, ^{223}Ra/^{228}Ra, and ^{224}Ra/^{228}Ra provide strong constraints of water mixing in the estuaries, embayments, and continental shelves, and can be used as proxies to evaluate the water residence time in these coastal waters.

Although comprising only ~7% of the world surface ocean, continental shelves and slopes play a disproportionately important role in carbon (C) and nitrogen (N) loadings (Hedges, 1992; Stukel et al., 2015), and contribute 14–30% of the oceanic PP (Cao et al., 2011; Gattuso et al., 1998). The C and N inputs include those derived from SGD (Liu et al., 2012, Q. Liu et al., 2014b), sediments (Cai et al., 2015), atmospheric deposit (Kim et al., 2014; Wang et al., 2012), coastal upwelling (Dugdale et al., 1990; Stukel et al., 2015), typhoon-derived nutrient injection (Lin et al., 2003), and mesoscale eddies (McGillicuddy et al., 1998, 2007). The exogenous nutrient fluxes to the continental margin will sustain the primary production in the euphotic zone. The PP supported by exogenous nutrient loadings is therefore called new production (Dugdale & Goering, 1967). Oceanographers have made efforts to depict the biogeochemical-physical processes that influence the PP and new production in the continental shelves. However, there are few studies that have looked into the linkage of SGD-derived nutrient to new production.

The SCS is the world second largest marginal sea with an area of 3.5×10^6 km^2 (Cao et al., 2011). As a tropic oligotrophic ocean, the surface mixed layer of SCS is both scarce in N and P with N: P ratios <16, indicating a nitrogen limitation condition (Chen et al., 2004; Han et al., 2013; Wu et al., 2003). Nitrogen bioavailability is believed to limit the PP in the oligotrophic SCS (Ryther & Dunstan, 1971; Wu et al., 2003). In SCS and other tropical oceans, the conventionally accepted mechanisms such as mesoscale eddies, coastal upwelling, atmospheric deposit and typhoon-derived upwelling, and N_2 fixation by Trichodesmium are not sufficient to explain the observed new production (Kim et al., 2014; Lin et al., 2003). It is speculated that SGD may have induced large nutrient loadings to the continental shelf in the SCS. However, there are very limited studies to address the impact of the groundwater-borne nutrient on new production in the SCS.

This study aims to investigate the SGD and the associated nutrient loadings. Based on the obtained cruise CTD data, the upwelling characteristics of eastern Hainan shelf are presented. By establishing the radium mixing model, water residence time over the eastern Hainan shelf is obtained. Thereafter, a coastal upwelling coupled radium mass balance model is proposed to quantify the SGD in the study area. The groundwater-borne nutrient to the eastern Hainan shelf is therefore calculated. Combined with previous studies on the exogenous DIN inputs to the shelf, the impact of groundwater-borne DIN on new production of the continental shelf is evaluated.

2. Methodology

2.1. Geological, Hydrological, and Hydrogeological Settings

Hainan Island, located in the north part of the South China Sea, has a surface area of 35.4×10^3 km^2. The climate is dominated by seasonal monsoons, with northeast winds in the winter and southwest wind in the summer. The annual average temperature ranges from 22.8 to 25.8°C and annual rainfall from 961 to 2,439 mm. As shown in Figure 1a, annual rainfall increases from 1,200 mm yr^{-1} at the west coast to over 2,000 mm yr^{-1} at the east coast. There are 13 major rivers on the island, with a total discharge of 31×10^9 m^3 yr^{-1}. There are mainly five rivers that empty into the eastern Hainan shelf, which are Wanquan River, Longshou River, Taiyang River, Linshui River, and Wenjiao River (Figure 1a). Suspended particulate matter (SPM) in the river water generally ranges from 55 to 197 mg L^{-1}. The total riverine sediment load from the

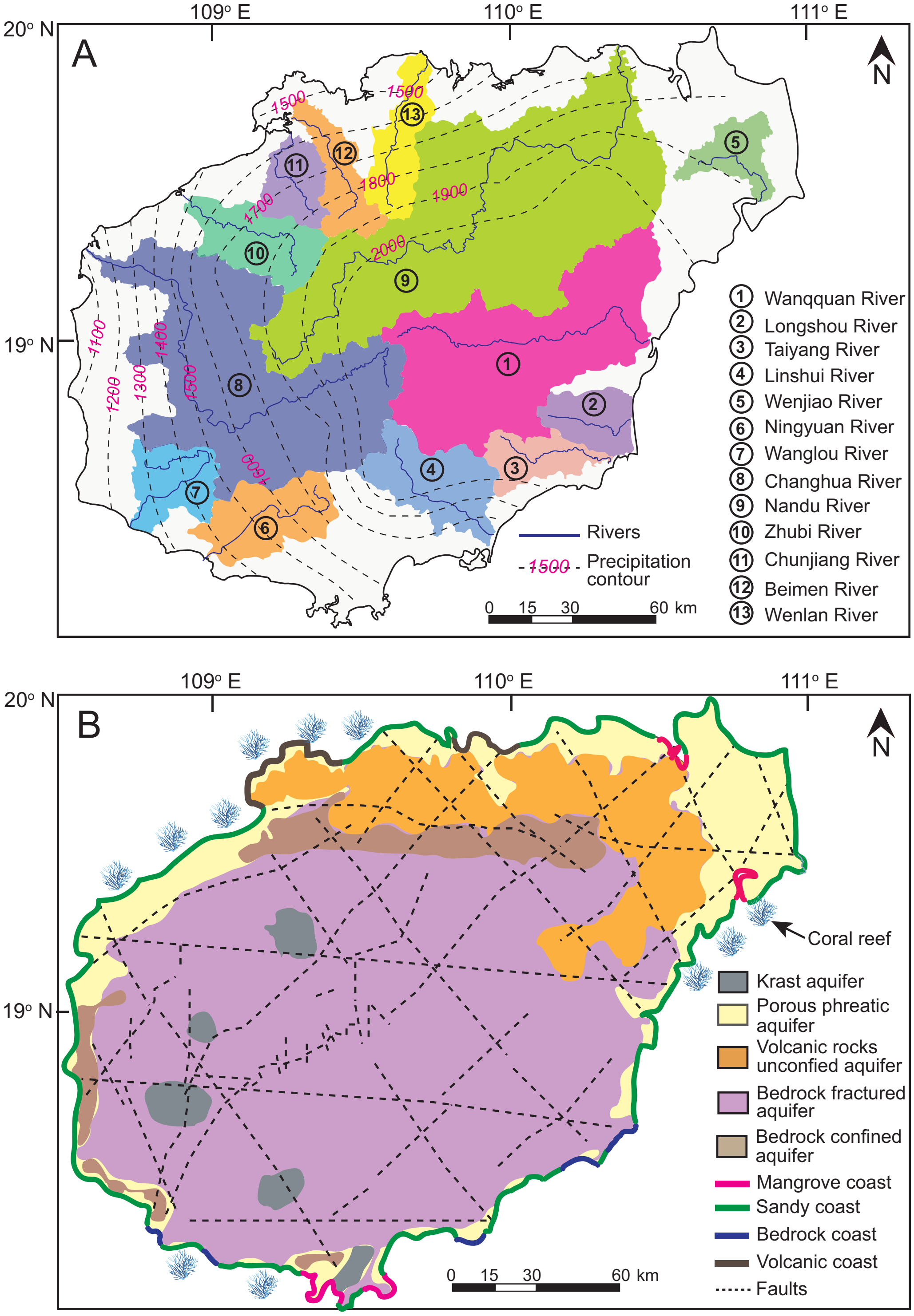

Figure 1. (a) Hydrological and (b) hydrogeological settings of the Hainan Island.

island is about 4 × 10^6 t yr^{-1} (Zhang et al., 2013). This study focuses on the SGD in the east coast of Hainan Island, which is featured by sand beaches and bars, lagoons and tidal channels, and estuaries. Controlled by the seasonal monsoon, the coastal circulation off the eastern coast is characterized by northeasterly current and coastal upwelling in the summer and southwesterly currents in the winter.

The hydrogeological setting of Hainan Island is shown in Figure 1b. The island is predominately consists of fractured unconfined aquifers in the inland areas and the porous phreatic aquifers at the coast. Faults are well developed all around the island, which may attribute to groundwater discharge (Shaban et al., 2005). The eastern coastal areas are dominated by sandy coast, occasional bedrock outcrop, and mangrove wetland (Figure 1b). These coastal settings are favorable for the groundwater discharge to coastal waters. According to Hainan Island regional hydrological report (Li & Lin, 1981), the shallow aquifer has a thickness ranging from 8.7 to 77.1 m. Groundwater table at the eastern island range from 1 to 3 m. The groundwater exploitation rate is 1.1×10^8 m^3 yr^{-1} over the eastern Hainan Island, which is much less than the natural groundwater recharge rate. Extensive infiltration from heavy rainfall and much less groundwater exploitation makes the north and eastern parts of the island to be a big groundwater reservoir (Li & Lin, 1981),

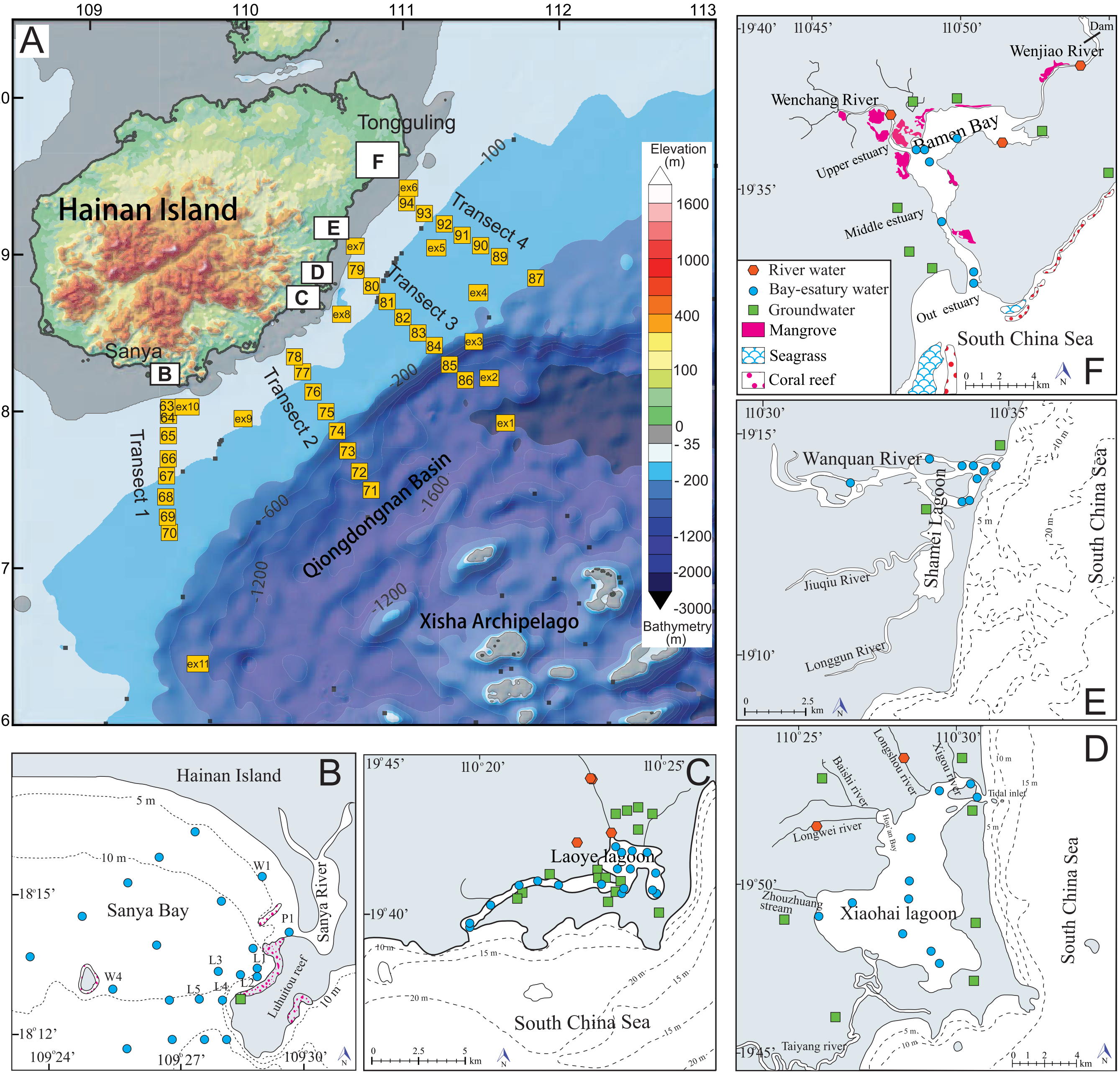

Figure 2. (a) Seawater sampling stations during the two summer cruises in 2012 and 2014, and sampling setting inland water in the Hainan coasts of (b) Sanya bay, (c) Laoye lagoon, (d) Xiaohai Lagoon, (e) Wanquan Estuary, and (f) Wenchang estuary.

providing source of fresh SGD to the eastern Hainan shelf (Zhou, 2005). The eastern Hainan shelf is adjacent to Qiongdongnan basin (Figure 2a). The most important physical oceanographic feature for the eastern Hainan shelf is summertime coastal upwelling off eastern Hainan, or Hainan eastern upwelling (HEU). HEU is formed due to the synergistic effect alongshore wind, wind stress curl-induced Ekman pumping, and the alongshore topographic variations (Hu & Wang, 2016; Jing et al., 2009, 2015; Lin et al., 2016a, 2016b; J. Su et al., 2011, 2013). The coastal upwelling, as a key physical driving force on nutrients and phytoplankton, will exert a profound impact on the oceanic primary productivity (Zhang et al., 2015).

During 2006–2011, the project of "land-sea interactions along coastal ecosystems of tropical China: Hainan" or LANCET, was carried out to investigate the land-sea interaction in the tropical areas, using eastern coasts of Hainan Island as an example. This project focused on the studies of land based fluxes and coastal hydrodynamics and their impacts on the coastal biogeochemical processes and the ecosystems such as coral reef, mangroves, and seagrass bed (Figure 2). The study area by LANCET covers from Tongguling in the north to Sanya Bay in the south (Figure 2a). There are several estuaries, bays, and lagoons located at the eastern coasts. The project studied the SGD and the derived nutrient loadings to these coastal bays and lagoons (Ji et al., 2012; Li et al., 2014; Liu et al., 2011; N. Su et al., 2011; Wang & Du, 2016). Extended SGD study by Wang et al. (2014) revealed that SGD serves as a significant contributor to the acidification of coral reef system in Sanya Bay at the southeast coast of Hainan Island. The fulfillment of LANCET and other groundwater related works along the eastern Hainan coasts provide valuable data set and background for further SGD studies in Hainan Island over regional and continental shelf scales.

2.2. Sampling and Analysis

The radium sampling was taken during two summer cruises on *R/V Shiyan III* in 2012 and 2014. In 2012, only 10 surface water radium samples were taken at the end of the cruise. The main sampling activities were conducted in the *R/V Shiyan III* in August–September 2014 (Figure 2a). Salinity, temperature, and conductivities were recorded with conductivity, temperature, and depth (CTD) probes (Seabird SBE 911) equipped on rotted multilevel sampler. Generally, a large volume of seawater (200–1,000 L) was pumped and filtered through 0.5 μm filter cartridges and stored in four marked 1.25 ton water tanks that were fixed on the board. The filtered water then passed through the columns containing 15–20 g MnO_2 fiber driven by gravity (Moore, 1976). The extraction efficiency test was done by connecting two fiber columns in series for the first station during each cruise. The flow rate ranged from 0.5 to 1.5 L min^{-1}, allowing complete extraction of dissolved radium. The mean extraction time ranged from 4–6 h for each sample. The radium samples were then delivered to China Geoscience University (Beijing) for radium measurements. The seawater water samples were filtered through 0.2 μm filter (Waterman, Co), and immediately frozen in the freezer on board. Salinity and temperature were recorded with an interval of 1 m for each CTD cast.

Due to significant decay loss, ^{224}Ra of the samples was not measured. ^{223}Ra was measured with RaDeCC as described in Luo et al. (2014). ^{226}Ra was measured with RAD 7 (Durridge, Co) by measuring ^{222}Rn under secular equilibrium with ^{226}Ra (Kim et al., 2001; Lee et al., 2012). ^{228}Ra was measured based on the ingrowth of ^{228}Th after storing the fiber for more than 9 months (Charette et al., 2015; Luo & Jiao, 2016; Luo et al., 2017). The uncertainties for ^{223}Ra and ^{228}Ra measurements are 10–20% and 7–12%, respectively. The uncertainties for ^{226}Ra measurement are 10–25%. DIN (the sum of NO_3^-, NO_2^-, and NH_4^+) and DIP were measured with Flow Injection Analysis (FIA) immediately after the cruise in the School of Biological Science, HKU. The detection limits for DIN and DIP are 0.03 and 0.01 μM, respectively.

Besides the field data from the cruises, the inland groundwater data are sourced from the previous publications (Jahnke et al., 2000; Li et al., 2014; Liu et al., 2011; N. Su et al., 2011; Wang et al., 2014; Wang & Du, 2016). Along the east coast, five coastal areas (sites B–F in Figure 2) have groundwater data of radium isotopes and nutrients from previous studies. These data can be used as representative of groundwater endmember of SGD (Figures 2b—2f). Details of these data are presented in supporting information Table S1.

2.3. Water Residence Time Estimation With ARs

The ARs of radium isotopes provide constraints to estimate the water residence time (WRT) over the continental shelves. In this study, WRT is represented by radium apparent age, which is the aging time of water from Ra sources. The basic concept is that large-scale radium input along the coastal line is akin to a purposeful trace release, with short-lived isotopes providing the rate of dispersion based on their decay as these nuclides mixing away from the sources (Charette et al., 2001; Moore, 2000). Since the water residence time of eastern Hainan continental shelf is expected to be longer than the half-life of ^{224}Ra, the ARs of ^{223}Ra/^{228}Ra are used to estimate the water residence time (Charette et al., 2001; Liu et al., 2012). Previous studies also suggested that HEU is influenced by alongshore current (Chu et al., 1998; Fang et al., 2002; Hu et al., 2000; Qu et al., 2000). However, the alongshore current in HEU is more intensified during the winter season due to the impact of northwestern winter monsoon. The sampling period is in summer and therefore, this study does not consider the mixing process induced by alongshore currents. This assumption is reasonable because previous studies have shown that currents perpendicular to the coastline other than alongshore current is dominant in HEU during the summertime (Hu & Wang, 2016; Jing et al., 2011, 2015; Lin et al., 2016a, 2016b; J. Su et al., 2011, 2013). Based on oceanographic settings and dominant radium sources, two scenarios are considered when deriving water residence time of upper layer of HEU with radium isotopes: with and without influences of coastal upwelling. For the off upwelling zone, the water residence time is calculated according to the following equation as described elsewhere (Liu et al., 2012; Moore, 2000)

$$\left[\frac{ex^{223}Ra}{ex^{228}Ra}\right]_{SW}=\left[\frac{^{223}Ra}{^{228}Ra}\right]_{GW}\times e^{-\lambda_{223}Tw} \tag{1}$$

where *ex* represents the excesses of ^{223}Ra and ^{228}Ra in inner shelf water relative to the open seawater. Subscripts *SW* and *GW* denote seawater and groundwater, respectively. T_w (day) is the water residence time; λ_{223} (d^{-1}) is the decay constant of ^{223}Ra. Notably, equation (1) is solely based on groundwater ages in surface ocean. The equation is valid under the following assumption: (1) there are no other main radium sources except for groundwater sources from coastline during radium transport in surface water. This assumption is reasonable as the following discussion shows that groundwater-borne radium is 1–2 orders of magnitude larger than riverine and sedimentary inputs; (2) the system is under steady state, which is valid for HEU.

For the upwelling zone, surface water is rapidly replaced by subsurface water. Since radium input to surface water is dominated by subsurface radium input, the residence time is therefore the functions of ARs of the subsurface water. According to Moore (2000) and Moore et al. (2006), WRT of surface water in the upwelling zone can be written as

$$T_U=\left[\left(\frac{^{223}Ra}{^{228}Ra}\right)_{Sub}-\left(\frac{^{223}Ra}{^{228}Ra}\right)_{U}\right]\Big/\left(\left(\frac{^{223}Ra}{^{228}Ra}\right)_{U}\times\lambda_{223}\right) \tag{2}$$

where $\left(\frac{^{223}Ra}{^{228}Ra}\right)_{Sub}$ is the ARs of ^{223}Ra/^{228}Ra in the input water, or the subsurface water in the inner shelf (Liu et al., 2012; Moore, 2000; Moore et al., 2006); $\left(\frac{^{223}Ra}{^{228}Ra}\right)_{U}$ is the ARs of ^{223}Ra/^{228}Ra in the surface seawater in the upwelling zones. Usually, the results of the residence time are mainly dependent on the ARs of ^{223}Ra/^{228}Ra in the subsurface water (Liu et al., 2012). The uncertainties of WTR and its dependence on the input variable will be further discussed in section 4.5.

2.4. Sedimentary Radium Input

The sedimentary radium input can be derived from the biophysical processes such as diffusion, physical mixing, bioirrigation, and bioturbations (Luo & Jiao, 2016; Luo et al., 2017; Moore et al., 2011). The sedimentary radium input (F_{sed}) can be estimated with the following equation

$$F_{sed}=P_{22i}\times\theta\times\sqrt{\frac{(D_{dis}+K_{22i}\times D_{mix})\times\lambda_{22i}}{1+K_{22i}}} \tag{3}$$

where P_{22i} (dpm per L^{-1} sediment) and K_{22i} are the sedimentary production rate and adsorption coefficient rate of nuclide *i*, θ is the sediment porosity, D_{dis}(m^2 s^{-1}) is the sedimentary dispersion coefficient for water movement through sediments due to bioirrigation and physical forces, and D_{mix}(m^2 s^{-1}) is the sedimentary mixing coefficient.

2.5. Radium and Nutrient Supply From Coastal Upwelling

The eastern Hainan shelf is intensively influenced by coastal upwelling, which delivers significant amount of nuclides and nutrients to the upper mixing layer. Generally, coastal upwelling in the eastern Hainan comprises of two components: (1) Ekman transport (v_{EK-T}) driven by along shore wind stresses; (2) Ekman pumping (v_{EK-P}) driven by cyclonic wind stress curl (Chavez & Messié, 2009; Hu & Wang, 2016; Liao et al., 2016; Messié et al., 2009). Ekman transport is speculated to occur within the Rossby radius of deformation (Allen, 1973; Bakun & Nelson, 1991). The Rossby radius is taken to be 55 km for most western boundary upwelling system at 19°N (Chelton et al., 1998; Liao et al., 2016). Ekman pumping is developed within an offshore width of 150 km. The nuclides and nutrients supply to the upper mixing layer by the coastal upwelling can be estimated with the following equation (Chavez et al., 1989; Chavez & Messié, 2009; Chavez & Toggweiler, 1994; Messié & Chavez, 2015; Messié et al., 2009).

$$F_{DIN_U} = v_{EK-T} \times [Ra_{D_{EK}} \text{ or } DIN_{D_{EK}}]_{Rossb} + v_{EK-P} \times [Ra_{D_{EK}} \text{ or } DIN_{D_{EK}}]_{150km} \tag{4}$$

where $[Ra_{D_{EK}} \text{ or } DIN_{D_{EK}}]_{Rossb}$ and $[Ra_{D_{EK}} \text{ or } DIN_{D_{EK}}]_{150km}$ are the average concentrations of radium or DIN below Ekman depth within Rossby radius of deformation and in a 150 km wide coastal region, respectively.

2.6. SGD Estimation with Radium Mass Balance Model

Under steady state, radium inventories in the seawater of continental shelves are sustained by various radium sinks and sources. Under the scenario with coastal upwelling, a radium mass balance model is setup for the mixing layer over the continental shelf

$$F_{mix} = F_R + F_{sed} + F_{SPM} + F_{SGD} + F_U \tag{5}$$

where F_{mix}, F_R, F_{sed}, F_{SPM}, F_{SGD}, and F_U denote oceanic radium mixing loss, radium riverine input, radium input derived from sedimentary processes from the seabed areas within the bathymetry of Ekman depth, input of radium from SPM desorption, SGD-derived radium inputs into the mixing layer through the seabed areas within the Ekman depth, and radium loading by coastal upwelling.

2.7. Estimation of Fresh SGD

Both Darcy's law and watershed recharge approach are used to quantify the fresh SGD to the eastern Hainan shelf. Fresh SGD based on Darcy's law can be written as (De Sieyes et al., 2008; Fetter & Fetter, 2001; Santos et al., 2009b),

$$Q_F = L_c \times (-K_h) \times \frac{dh}{dw} \times L_w \tag{6}$$

where L_c (m) is the length of eastern Hainan coastal line, K_h (m d^{-1}) is the horizontal hydraulic conductivity, and $\frac{dh}{dw}$ is hydraulic gradient at the coasts of Hainan Island. L_w (m) is the maximum width of fresh groundwater seepage face and can be expressed as (Bokuniewicz, 1992; Taniguchi et al., 2006),

$$L_w = 4 \times H_a \Big/ \sqrt{\frac{K_v}{K_h}} \tag{7}$$

where H_a (m) is the thickness of the shallow aquifer system and K_v (m d^{-1}) is the vertical hydraulic conductivity.

Watershed recharge approach is based on water budget within a catchment behind the coastal areas (Cambareri & Eichner, 1998; Kim et al., 2003; Kroeger et al., 2007; Lee et al., 2012; Luo & Jiao, 2016; Oberdorfer, 2003; Santos et al., 2009a). In this study, fresh SGD estimate based the watershed recharge is expressed as

$$Q_F = P \times S \times \alpha - Q_r - Q_{extract} \tag{8}$$

where P (mm yr^{-1}) is the annual precipitation in the catchment. S (m^2) is the recharge areas. Q_{river}(m^3 yr^{-1}) and $Q_{extract}$(m^3 yr^{-1}) are discharge to the SCS from the five main rivers in the eastern coast, and the exploitation rate of groundwater, respectively, α_i is the infiltration coefficient of the aquifer in eastern Hainan Island.

3. Results

3.1. Hydrography Based on Remote Sensing Data

High-resolution satellite data, including sea surface temperature (SST), sea surface chlorophyll (SSChla), and surface current distributions were used to evaluate the spatial variation of these surface parameters in eastern Hainan shelf. Monthly SST and SSChla were acquired from the NASA's Moderate Resolution Imaging

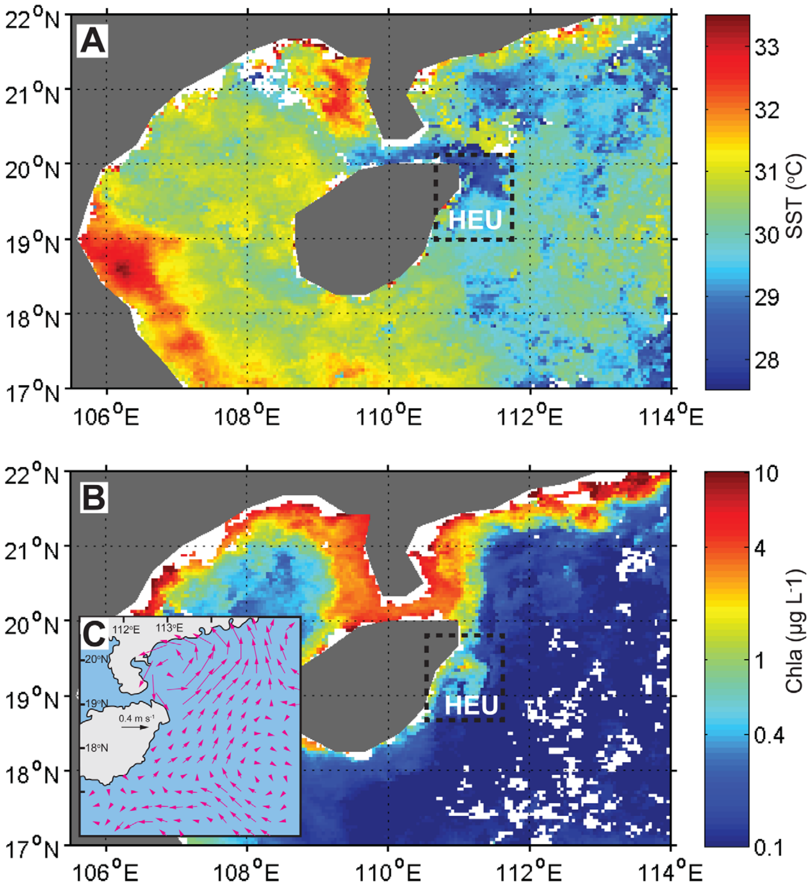

Figure 3. The physical oceanographic settings of the study area during the sampling period in September 2014. (a) Sea surface temperature (SST) distributions from MODIS-AQUA; (b) the remote sensing data of chlorophyll obtained from MODIS-AQUA; (3) surface current velocity distribution obtained from OSCAR satellite.

Spector-radiometer data observed by the aqua satellite (MODIS-Aqua). Surface velocity fields (0.3° × 0.3°) were obtained from multisatellite altimeter (TOPEX, JASON-1, ERS-2, ENVISAT, and GFO) and scatterometer data distributed by the NOAA's Ocean Surface Current Analysis-Realtime (OSCAR) program. The average SST distribution of September 2014 is shown in Figure 3a. Obviously low temperature zone is observed in the eastern of Hainan Island, indicating the existence of HEU. The SSChla distribution also shows that the HEU zone is rich in chlorophyll, suggesting much higher PP (Figure 3b). The distribution of sea surface velocity shows that surface current curls distributed at the north and eastern of Hainan shelf, which potentially leads to coastal upwelling (Figure 3c).

3.2. Hydrographic and Physical Oceanographic Dynamics

Spatial distributions of field data of seawater temperature (T), salinity (S), and density abnormal (σ) at the layers of 5, 25, 50, 75, and 100 m are shown in Figure 4. T ranges from 29.4 to 30.2°C in the upper layer, and gradually declines to 26–30°C at 25 m, 22–25°C at 50 m, 19–22°C at 75 m, and 18–20.5°C at 100 m. The nearshore seawater has relatively low T compared to that in the open seawater, suggesting the effect of coastal upwelling of Ekman transport driven by SW along shore wind. At the northeastern of the area, there is a lower temperature zone with a temperature about 0.3–0.5°C lower than that in the adjacent areas. The low temperature zone expands at 25 m and reaches the maximum at the depth of 50 m. At the layers of 75 and 100 m, the lower temperature zones are reduced to the northeastern zone. The lower temperature zones at the nearshore coastal areas are mainly caused by the Ekman transport driven by alongshore wind during the summer seasons, and the lower temperature core at the northeastern coastal was speculated to be resulted from Ekman pump driven by the cyclonic wind stress curl (Jing et al., 2009, 2015; Lin et al., 2016b; J. Su et al., 2011, 2013). Salinity and density anomaly gradually decline with depths in each layer. The spatial

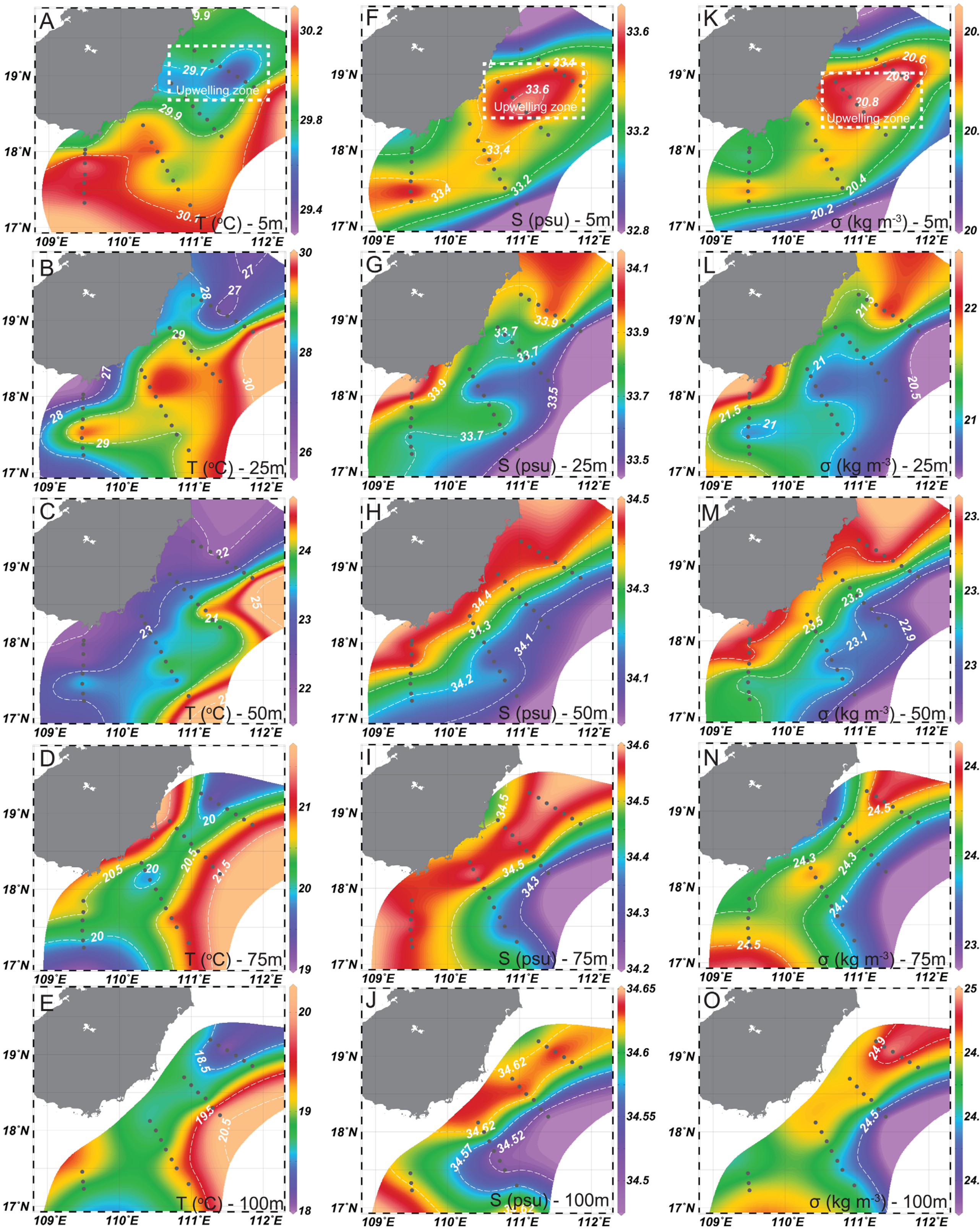

Figure 4. Distributions of salinity, temperature, and density anomaly in the layers of 5, 25, 50, 75, and 100 m obtained during cruise of September 2014.

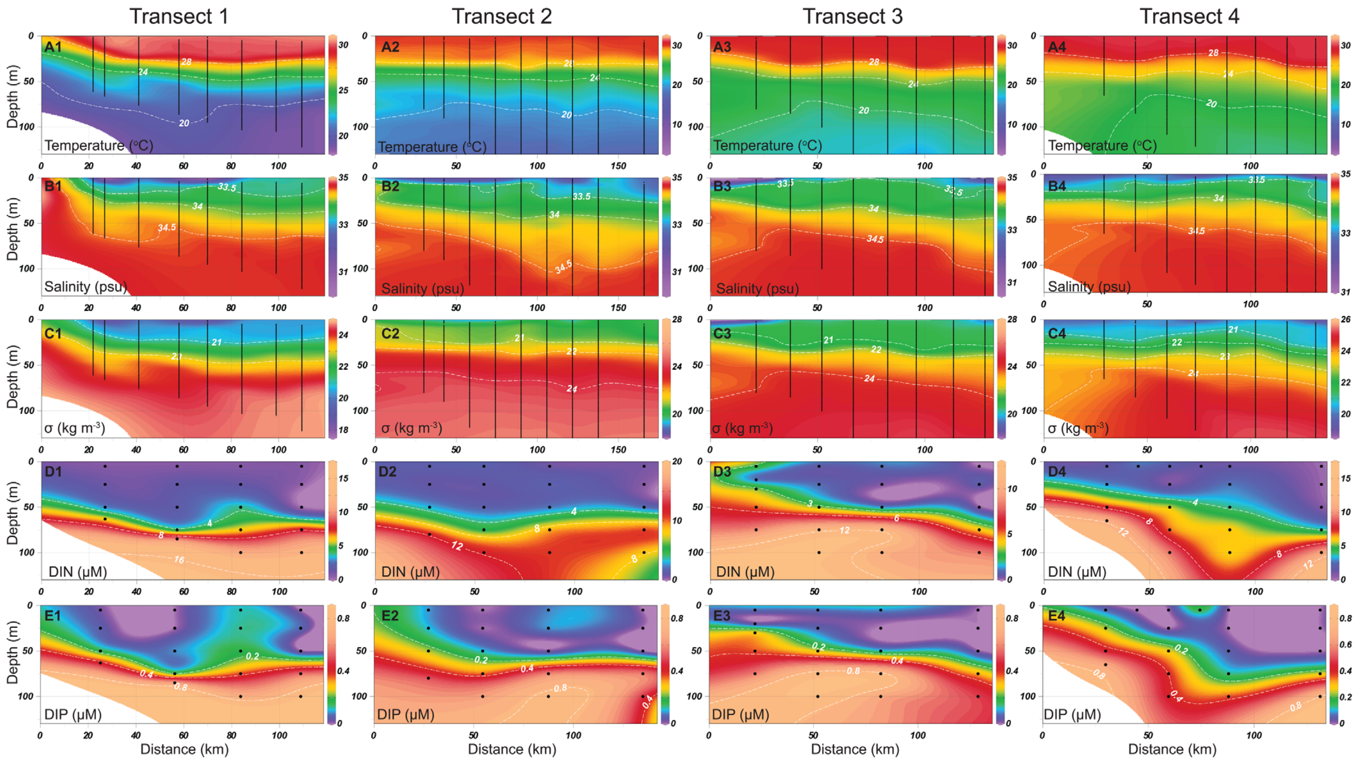

Figure 5. Vertical structures of salinity, temperature, and density anomaly of four sampling transects obtained during cruise of September 2014. The rectangles indicate the coastal upwelling zones driven by Ekman pumping.

distributions of S and σ are generally opposite to the temperature distributions at all the sampling layers (Figures 4f—4o). The higher salinity and density zones are mostly located at the northeastern areas off Hainan Island at the depth of 5 m, with a zonal salinity and density anomaly of 33.8 psu and 20.8 kg m^{-3}, respectively (Figures 4f and 4k). The relatively lower salinity zone close to the coastal line could be a result of terrestrial runoff and SGD (Lin et al., 2016b; J. Su et al., 2011). The high salinity zone expands to most areas of inner shelf at the depths of 50 m, indicating intensified upwelling.

The vertical structures of T, S, and σ are shown in Figure 5. Temperature of transects 1, 3, and 4 shows obvious upwelling at the nearshore areas, while transect 2 is almost stratified with a depth of 35 m (Figures 5a1–5a4), suggesting the mixing layer depth (MLD) is about 35 m during the sampling period. Salinity and density anomaly of transects 1 and 2 are higher at the nearshore areas, indicating the upwelling of more saline subsurface driven by Ekman transport. Salinity and density anomaly of transects 3 and 4 are relatively higher at the distance of 50–100 km from the coastal line, indicating the upwelling of Ekman pumping driven by cyclonic wind stress curl (Figures 5b3–5b4 and 5c3–5c4). This phenomenon is consistent with the spatial distributions of S and σ. The spatial distributions and vertical structures of T, S, and σ well indicate the development of HEU, which has been widely reported in the previous studies (Jing et al., 2011, 2015; Lin et al., 2016a, 2016b; Song et al., 2012; J. Su et al., 2011, 2013; Wang et al., 2013).

The isopycnal graph of T-S shows the mixing of different water masses (Figure 6a). Seawater in the upper layer (<35 m) of eastern Hainan shelf are generally influenced by three water masses: (1) inland groundwater and surface water of river, estuary, and bay, (2) open sea surface water, and (3) open sea subsurface upwelling water. Groundwater and estuary water is normally less saline compared to the open seawater (supporting information Table S1 and Figure 6a). The open sea surface water is characterized by high T, and relatively high S and medium σ (Figure 6a). The upwelling water is mostly with lower T, and high S and σ (Figure 6a). The surface water of the shelf is mostly controlled by the processes of mixing and upwelling, with less influence of inland water bodies, which is similar to the findings reported by Lin et al. (2016b) and J. Su et al. (2011) with three end-member mixing models.

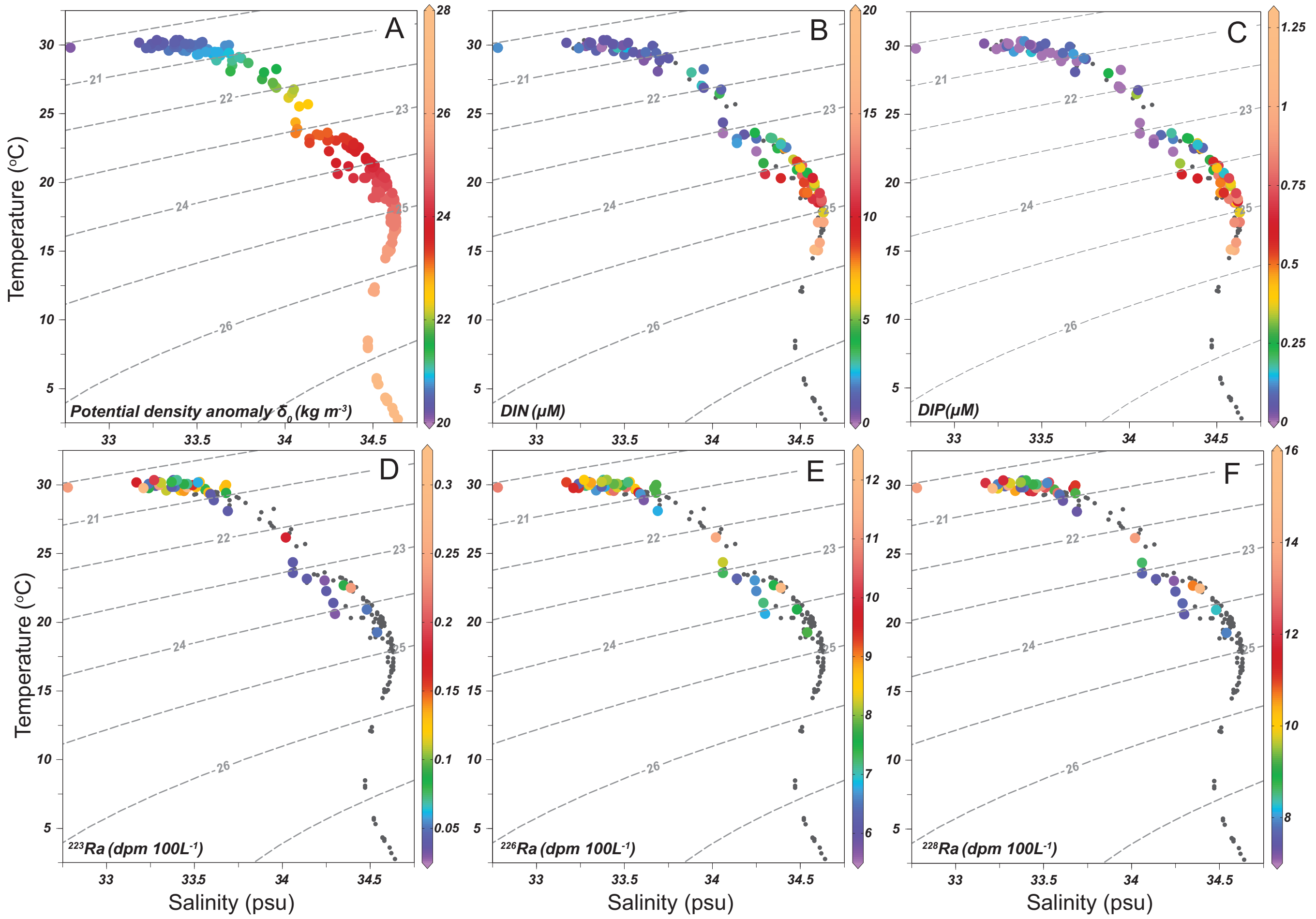

Figure 6. The isopycnal graph of (a) T-S, and contours of (b) DIN, (c) DIP, (d) ^{223}Ra, (e) ^{224}Ra, and (f) ^{228}Ra on the isopycnal graph of T-S.

3.3. Nutrients Dynamics in Different Water End-members

Nutrient (DIN and DIP) distributions along the four sampling transects are shown in Figures 5d1–5e4. DIN and DIP in the four transects range from 0 to 20 μM, and 0 to 1.1 μM, respectively, which are in line with the previous studies in the same sea areas (Song et al., 2012; Zhang et al., 2015). The surface seawater of tropic oceans is mostly oligotrophic, due to the new production consummation by the phytoplankton (McGillicuddy et al., 1998, 2007; Wong et al., 2007). The nutricline was mainly located about 35 m in the eastern Hainan shelf, with relatively smaller values at the inner shelf and larger values at the out shelf areas. This phenomenon also suggests the nutrient is supplied to the euphotic zones by the coastal upwelling (especially by Ekman transport) at the nearshore areas, as indicated in other biogeochemical studies of the coastal upwelling systems (Chavez & Messié, 2009; Liao et al., 2016; Messié & Chavez, 2015; Messié et al., 2009). DIN and DIP are further plotted on the T-S isopycnal to reveal nutrient dynamics in different water masses (Figures 6b and 6c). The surface water is mostly depleted in DIN and DIP, while the subsurface water is concentrated in DIN and DIP. Nutrient from the upwelled subsurface water is a significant nutrient source for inner shelf surface water. The nutrients supplied to the eutrophic zones by the costal upwelling will greatly enhance the new production and caused much higher PP. The relation of nutrient versus groundwater is shown in Figures 7a and 7b. DIN is well correlated with DIP, with a relation of DIN = 14.6 × DIP + 0.7 (Figure 7c). The slope of DIN versus DIP is lower than 16. This ratio is an appropriate ratio for phytoplankton growth. In the groundwater end-member, DIN ranges from 4 to 1,779 μM, with an average of 478.2 μM (n = 30) and DIP from 0.04 to 7.6 μM, with an average of 0.5 μM (n = 18). For the river and estuary water, the nutrient concentration and dynamics are summarized in supporting information Table S1, based on various nutrient studies. N: P ratios in the groundwater, river water, and estuary water are much higher than

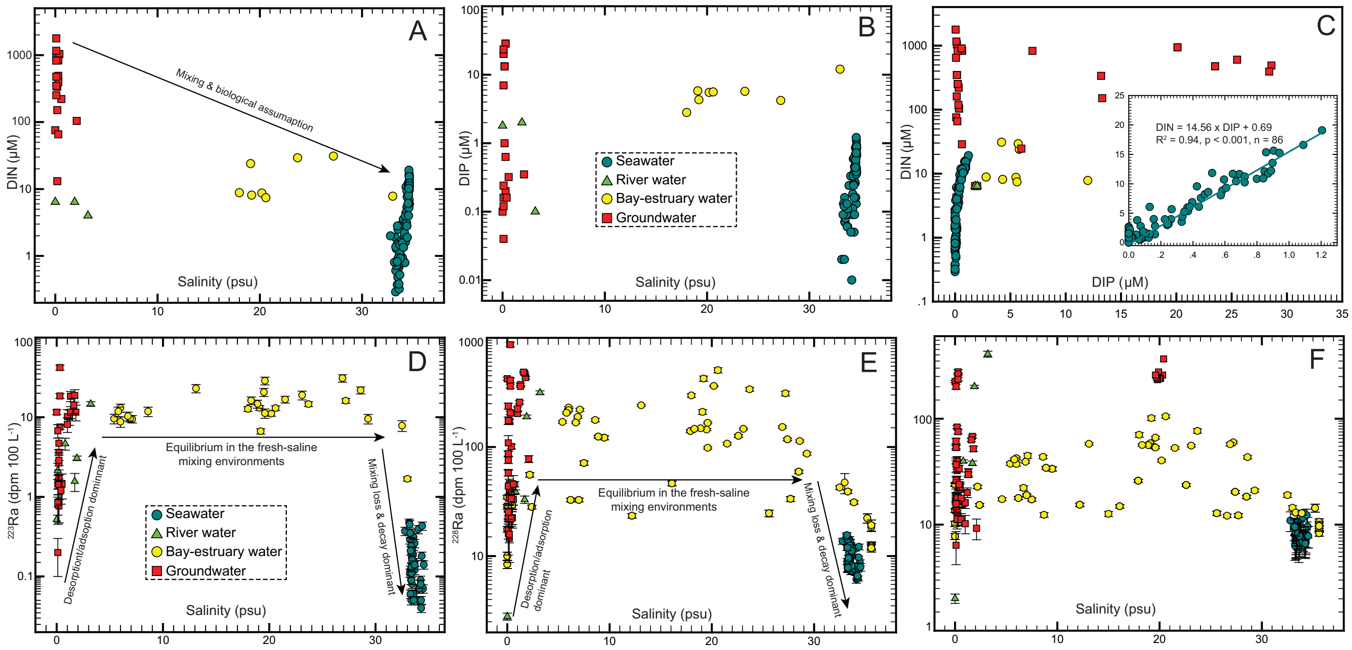

Figure 7. Spatial distributions of (a) ^{223}Ra, (b) ^{226}Ra, (c) ^{228}Ra during the two sampling cruises, and (d) the calculated ^{223}Ra/^{228}Ra ages. The rectangles indicate the upwelling zone driven by Ekman pumping.

16, and much larger than those of seawater, indicating these inland water bodies serve as an important DIN source to coastal seawater.

3.4. Radium Isotopes in Different Water Members

The spatial distributions of radium isotopes in the seawater are shown in Figures 8a—8c. Generally, the inner shelf water is much concentrated in radium isotopes compared to the open seawater. The excesses of radium isotopes in the inner shelf water are caused by the high radium loadings from sedimentary processes, SGD, and coastal upwelling input. From nearshore to the open seawater, respectively, the activities of ^{223}Ra range from 0.03 to 0.3 dpm 100 L^{-1}, ^{226}Ra from 5.9 ± 1.1 to 13.7 ± 1.1 dpm 100 L^{-1}, and ^{228}Ra from 6.1 ± 0.6 to 15 ± 0.9 dpm 100 L^{-1}. Activities of ^{226}Ra and ^{228}Ra almost reach constant values of 5.9 and 6.2 dpm 100 L^{-1}, respectively, in the seawater $>$150 km off the island shoreline. Activities of ^{223}Ra are almost below detection limits ($\approx$ 0.003 dpm 100 L^{-1}) in the open seawater. The radium spatial distribution is speculated to be mainly controlled by SGD, decay, and mixing processes, as being concluded by previous studies elsewhere (Burt et al., 2014; Hancock et al., 2006). The excesses of radium isotopes in the inner shelf for ^{226}Ra and ^{228}Ra allow these nuclides as ideal tracers to be used to quantify the SGD within the coastal shelf. There are obvious radium hotspots at the coastal upwelling zone driven by Ekman pumping. Similar high radium activities were also observed at the upwelling zones of north SCS shelf (Liu et al., 2012). Specifically, high radium activities are also overserved at the immediate water out of Bamen Bay, Sanya Bay, and Wanquan River estuaries (Figure 7), suggesting the radium loadings from terrestrial runoff. Vertically, radium isotopes are enriched in the bottom shelf water compared to the surface water for the inner shelf water (Figure 10), suggesting large sedimentary and SGD-derived inputs. Radium isotopes increase with the depth for inner shelf water, but show no obvious increase with depth in the open seawater (Figure 10). The vertical distribution is consistent with the observations of radium profiles in SCS and elsewhere (Cai et al., 2002; Charette et al., 2015; Chen et al., 2010; Liu et al., 2012; Rodellas et al., 2015). Radium isotopes are contoured on the T-S isopyicnal graphs to further investigate the relations of radium with these hydrographic parameters. The nearshore inner shelf water is usually characterized by high radium and T, and low S and σ, suggesting that radium are mainly from terrestrial sources such as SGD and fluvial loadings. The open surface water contains much less radium isotopes. The subsurface water of inner shelf is concentrated in ^{223}Ra, ^{228}Ra, and ^{226}Ra (Figures 6d–6f). This suggests radium loadings from the seabed in form of SGD and sedimentary processes as bioirrigation, and pore water diffusion, as indicated in other radium studies of continental shelf (Burt et al., 2014; Liu et al., 2012, Q. Liu et al., 2014).

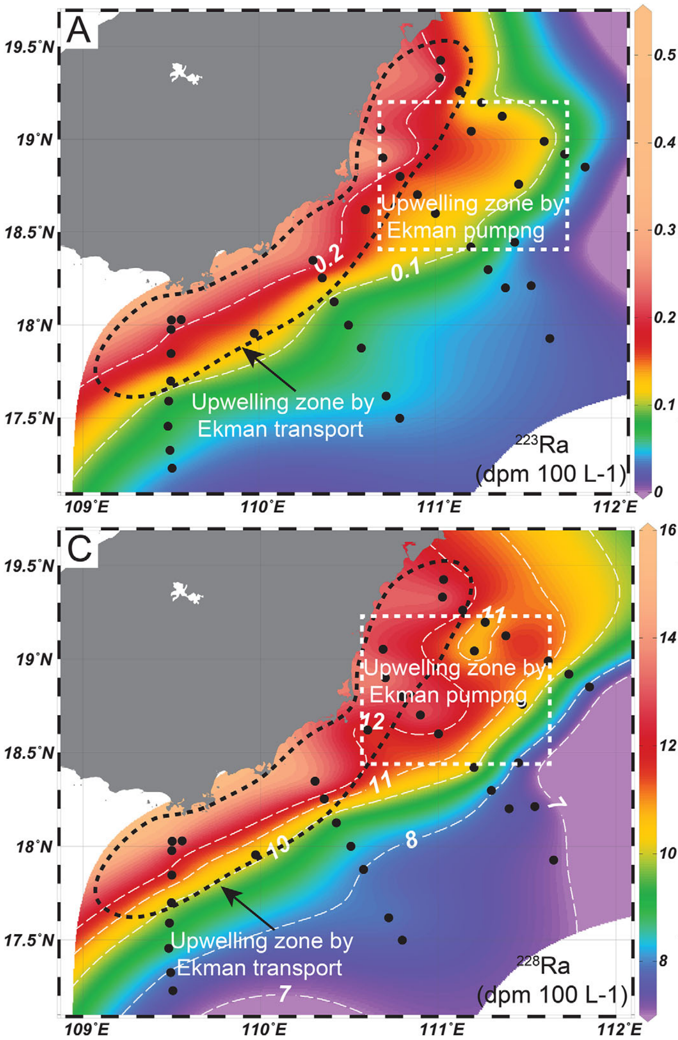

Figure 8. The relations of salinity versus (a) ^{223}Ra, (b) ^{228}Ra, (c) ^{226}Ra, (d) DIN, and (e) DIP in different water end-members, and (f) the relation of DIN versus DIP in different water end-members.

Radium isotopes in the groundwater end-member are summarized in supporting information Table S1. Activity of ^{228}Ra in the coastal groundwater ranges from 14.5 to 865 dpm 100 L^{-1}, with an average of 171 ± 13.8 dpm 100 L^{-1}, and ^{226}Ra ranges from 6.4 to 366 dpm 100 L^{-1}, with an average of 103 ± 67.9 dpm 100 L^{-1}. The relations of radium isotopes versus salinity are shown in Figures 7d—7f. Radium in coastal groundwater is mainly controlled by the adsorption/desorption processes. Hypersaline groundwater is usually enriched in radium isotopes due to high desorption rate. Fresh groundwater is depleted in radium nuclides, due to their high affinity to aquifer grains. Radium activities in river water have relatively wide ranges. Radium sorbed on SPM of fresh river water will be released when encountering saline environments. Seawater is much more depleted in radium isotopes compared to groundwater and bay-estuary water (Figures 7d—7f). The large difference of radium isotopes between different water end-members allows these nuclides to be ideal tracers to quantify SGD using the mass balance models.

4. Discussion

4.1. Water Residence Time

According to the spatial distribution of hydrographic parameter and radium isotopes (Figures 5 and 8), there is a zonal area with higher salinity and radium activities and low temperature off the northeastern coasts along transects 1 & 2. Relatively high radium isotopes are found in the upwelling zone. The ARs of

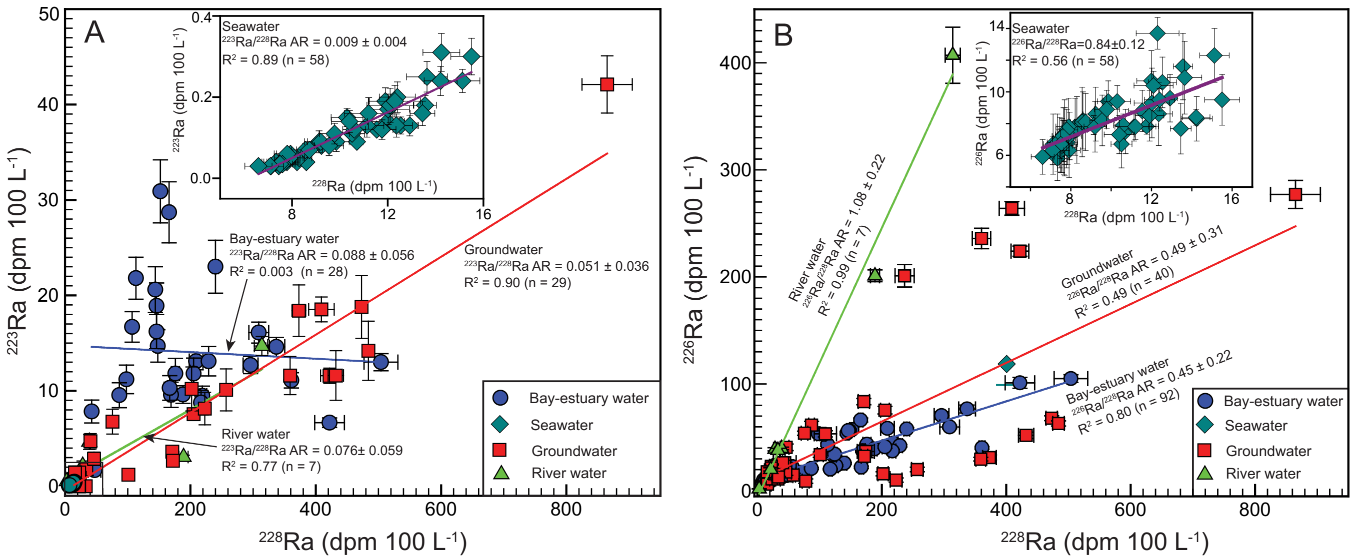

Figure 9. The relations of ^{228}Ra versus (a) ^{223}Ra and (b) ^{226}Ra in different water end-members.

^{223}Ra/^{228}Ra in the groundwater range from 0.9×10^{-2} to 1.2×10^{-1}, with an average of $(5.1 \pm 3.6) \times 10^{-2}$ ($n = 30$). The ARs of ex^{223}Ra/ex^{228}Ra in the seawater range from 0.005 to 0.037, within an average of $(1.9 \pm 0.9) \times 10^{-2}$ ($n = 43$) (Figure 9). Substituting the average ARs of ^{223}Ra/^{228}Ra in the groundwater and each value of ex^{223}Ra/ex^{228}Ra into equation (1), the water residence time is obtained to be 5.4 – 38.2 days, with an average of 18.7 days in the off upwelling zone. For the upwelling zone, water residence time needs to be calculated with equation (2). The ARs of ^{223}Ra/^{228}Ra in the surface water of upwelling zone range from 0.8×10^{-2} to 1.6×10^{-2}, with an average of $(1.1 \pm 0.2) \times 10^{-2}$ ($n = 11$). The ARs of ^{223}Ra/^{228}Ra (1.6×10^{-2}) for the subsurface water from Station 93 (*Sta. 93*) is used as the input water to calculate the water residence time at the upwelling zone, as suggested by Moore and Wilson (2005) and Liu et al. (2012). The upwelling zone has a water residence time of 5.7–14.8 days, with an average of 10.2 ± 3.0 days. Figure 8d shows the spatial distributions of water residence time. Water residence time is within a week in the nearshore areas, and increases toward the open seawater. The open seawater (>150 km) has water residence time more than 30 days. The average water residence time in the entire study area is calculated to be 16.9 ± 8.9 days. WRT of upwelling zone is smaller than that of off upwelling zone, indicating surface water of upwelling zone is refreshed more quickly. Similarly, Liu et al. (2012) obtained a WRT of 8.6 ± 6.7 days and 16.3 ± 10.3 days in the in the upwelling zone, and off upwelling zones of north South China Sea (NSCS). The obtained water residence time is well in line with the results of others studies in the NSCS shelf area (Liu et al., 2012), and well consistent with other radium based water residence time estimates in the marginal seas and continental shelves (Q. Liu et al., 2014; Moore, 2000, 2007).

4.2. The Estimate of the SGD

The mass balance model is established for the mixed layer above Ekman depth of the eastern Hainan shelf. The profiles of salinity, temperature, and density in *Sta. 87* (open sea) and *Sta. 93* (inner shelf) shows that the upper mixing layer is about 35 m during the summer season (Figure 10). The value is consistent with the Ekman depth as indicated by others studies in eastern Hainan shelf during the summer seasons (Zhang et al., 2015), and the Ekman depth is therefore taken to be 35 m in this study. Mass balance models of ^{226}Ra and ^{228}Ra are established above the Ekman depth of 35 m to quantify the SGD. As shown in Figure 11a, radium sources include riverine loadings, SGD-derived input, atmospheric deposit, sedimentary input and upwelling input, and radium is mainly lost via oceanic mixing processes. The activities of ^{226}Ra in river/estuary waters have a range of 2.0–407 dpm 100 L^{-1}, with an average of 32.9 ± 46.0 dpm 100 L^{-1}, and ^{228}Ra from 2.8 to 504 dpm 100 L^{-1}, with an average of 92.4 ± 98.8 dpm 100 L^{-1} (supporting information Table S1). The river/estuary discharge of the eastern Hainan coastline is 2.06×10^{7} m^{3} d^{-1} (Li et al., 2014; Zhang et al., 2013). Thus, the fluvial radium loading of ^{226}Ra and ^{228}Ra is estimated to be 2.2×10^{10} and 1.9×10^{10} dpm d^{-1}, respectively. Radium in the SPM is desorbed in the saline environment and the desorption rate is

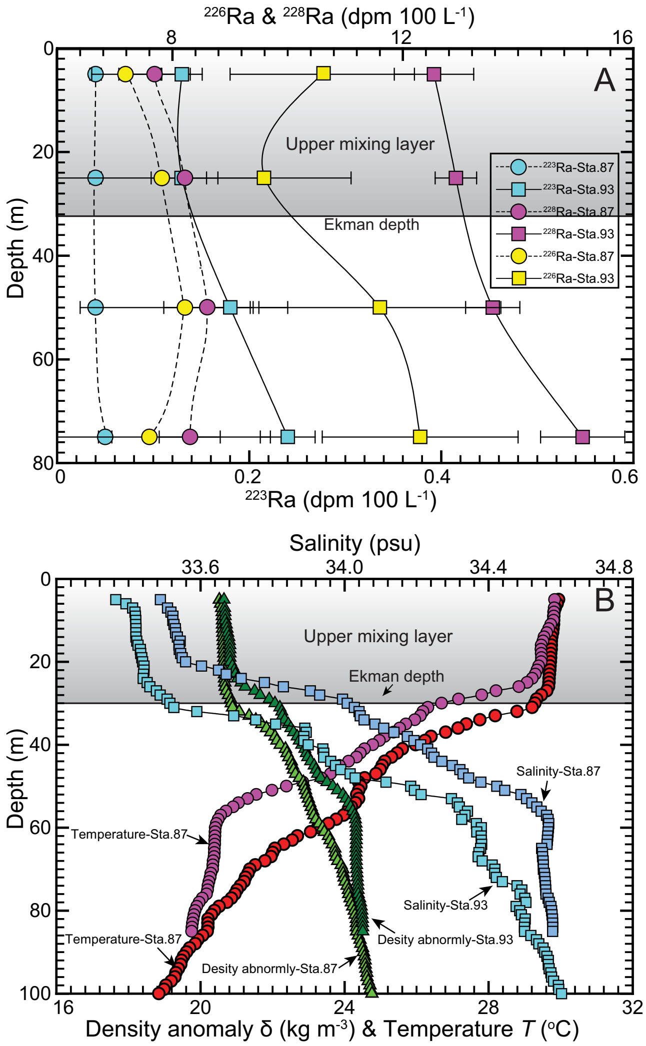

Figure 10. (a) The profiles of ^{223}Ra, ^{226}Ra, and ^{228}Ra and (b) temperature, salinity and density anomaly in the *Sta. 87* in the open seawater and *Sta. 93* in the inner shelf.

assumed to 2 dpm g^{-1} for both ^{226}Ra (Moore, 1996) and ^{228}Ra (Moore et al., 2008). The SPM deposit rate in the study area is 0.1 g m^{-2} d^{-1} (J. Liu et al., 2014). Therefore, the atmospheric deposit of radium to the study area is calculated to be 1.0 × 10^{10} dpm d^{-1}, respectively.

Accounting to equation (3), sedimentary radium input can be estimated with the constants of θ, λ_{22i}, D_{dis}, D_{mix}, and estimated values of K_{22i} and P_{22i}. The sedimentary input of ^{226}Ra is negligible, due to the much smaller value of λ_{226} and high adsorption rate (Luo & Jiao, 2016; Luo et al., 2017; Moore et al., 2011). θ, D_{dis}, and D_{mix} have the values of 0.4, 2.0 × 10^{-9} and 6.0 × 10^{-9} m^2 s^{-1} for typical marine sediment (D'Andrea et al., 2004; Green et al., 2002; Moore et al., 2011; Van Der Loeff, 1981). Activities of ^{228}Ra of surficial sediments in the NSCS shelf range from 0.9 to 3.3 dpm g^{-1}, with an average of 2.7 dpm g^{-1} (Liu et al., 2001, 2012). The density and porosity of marine sediment is 1.5 kg L^{-1} and 0.4, respectively (Luo et al., 2014). The leaching ratio of ^{228}Ra from marine surficial sediments is assumed to be 7% (Luo & Jiao, 2016; Moore et al., 2011). With sediment density, porosity, the radium composition and leaching ratio, the ^{228}Ra production rate is estimated to be 39 – 141 dpm per liter wet sediment, with an average of 116 dpm per liter wet sediment. The average ^{228}Ra activity in the coastal saline pore water is 171 ± 13.8 dpm 100 L^{-1} (Table 1). Thus, the sediment/water partition coefficient K is calculated to be from 20.5 to 74.2, with an average of 61.1. Combining the constants of θ, λ_{22i}, D_{dis}, D_{mix} with the estimated P_{22i} and K_{22i}, the sedimentary fluxes rate is calculated to be 2.2 – 7.5 dpm m^{-2} d^{-1}, with an average of 6.3 dpm m^{-2} d^{-1}. Considering the sediment surface area of above the bathymetry to be ≈ 9 × 10^9 m^2 at the earth Hainan shelf, sedimentary input is estimated to be 5.7 (0.7–6.8) × 10^{10} dpm d^{-1}. The upwelling rate derived from Ekman transport and Ekman pumping is estimated to be 0.14 and 0.07 Sv, respectively (Wang et al., 2013). The average ^{226}Ra and ^{228}Ra of 14.3 ± 1.1 and 11.7 ± 1.6 dpm 100 L^{-1} in subsurface waters (> 35 m) at *Sta. 93* are used to represent to source water of upwelling driven by Ekman transport. The average activities of ^{226}Ra and ^{228}Ra in subsurface waters of *Sta. 87* (> 35 m) in the open sea are 7.9 ± 0.3 and 8.5 ± 0.6 dpm 100 L^{-1}, respectively.

Water residence time ranges from 5.4 to 38.2 days, with an average of 16.9 days (n = 54) in the study area. Using the gridding method as detailed in supporting information and with the layer thickness to be the Ekman depth (= 35 m), the inventory of ^{228}Ra and ^{226}Ra activities in study area is calculated to be (1.7 ± 0.1) × 10^{14} dpm and (1.4 ± 0.2) × 10^{14} dpm for ^{228}Ra and ^{226}Ra, respectively, which is equivalent to 9.4 ± 0.6 and 7.8 ± 0.9 dpm L^{-1}, respectively. The seawater sample at *Sta. Ex1* (≈ 200 km offshore) is chosen to represent the open seawater end-member and the ^{228}Ra and ^{226}Ra activities of this sample are 6.6 ± 0.6 and 5.9 ± 1.1 dpm L^{-1}, respectively. The excesses of ^{226}Ra and ^{228}Ra for the inner shelf seawater in related to the open seawater is therefore calculated to be ≈ 2.8 and ≈ 1.9 dpm 100 L^{-1}, based on which the mixing loss of the ^{226}Ra and ^{228}Ra is calculated to be 2.1 × 10^{12} and 3.1 × 10^{12} dpm d^{-1}. After obtaining all the radium sinks and sources with the mass balance models, the SGD-derived ^{226}Ra and ^{228}Ra loadings are calculated to be 2.1 × 10^{11} and 7.4 × 10^{11} dpm d^{-1} (Table 1).

Radium activity in groundwater end-member is essential to estimate SGD in this study (Cho & Kim, 2016; Kwon et al., 2014; Moore et al., 2008). Regionally, radium in coastal groundwater may exhibit both geographical heterogeneity and salinity effect (Cho & Kim, 2016; Moore et al., 2008). Previous studies employ a gridding method, which indicates that geographical skewness of data distribution does not significantly affects radium groundwater end-member values (Cho & Kim, 2016; Moore et al., 2008). Salinity of groundwater shows more significant effects on radium activities in coastal groundwater. Since the dominant

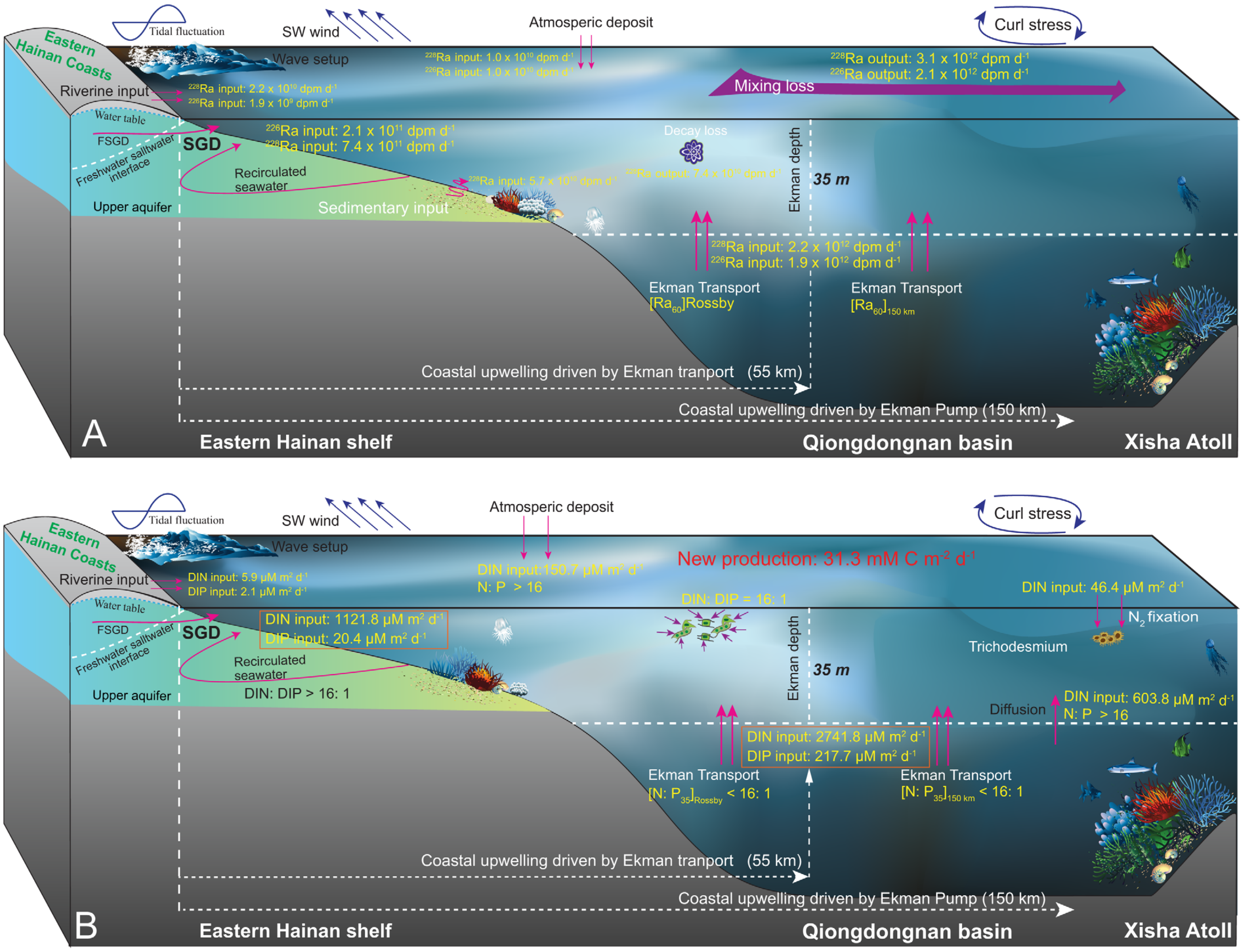

Figure 11. Schematic graphs of (a) radium sinks and sources and (b) nutrient dynamics in eastern Hainan upwelling system.

components of SGD is recirculated seawater (Table 1), and radium activities in groundwater with salinity of 10–30 psu may be more representative of groundwater discharging into the coasts. Thus, when calculating the final SGD, radium activities in groundwater with salinity of 10–30 are used to calculate the final SGD. In this study, the lognormal average of ^{226}Ra in groundwater with salinity of 10–30 psu is 245.4 ± 35.0 dpm 100 L^{-1}. Since there is few data of ^{228}Ra in groundwater with salinity of 10–30 psu, thus ^{228}Ra in saline groundwater was derived from the relation of ARs of ^{226}Ra/^{228}Ra $= 0.49 \pm 0.31$ ($R^2 = 0.49$, $n = 40$) (Figure 9), leading to an average ^{228}Ra activity of 519.4 ± 217.6 dpm 100 L^{-1}. Thus, based on the obtained ^{226}Ra and ^{228}Ra in saline groundwater end-member, SGD is finally calculated to be 1.4×10^8 and 8.1×10^7 m^3 d^{-1}, respectively. ^{226}Ra and ^{228}Ra models lead to similar SGD estimates, indicating the tenable results.

4.3. The Fresh SGD and the Comparisons

Fresh SGD can be estimated based on equation (6). The parameters used in the Darcy estimate are shown in Table 1. The length of the eastern Hainan coastline is ≈ 300 km. The hydrogeological parameter of K_h, $\frac{dh}{dw}$, and H_A for the eastern coastal area are retrieved from 1: 50,000 regional hydrogeological maps of Wen Chang, Wanning-Linshui, and Sanya sheets, and 1: 200,000 Hainan Island hydrological map (Li & Lin, 1981). The values of K_h in the eastern coasts range from 0.8 to 32 m d^{-1}, with an average of 8.3 ± 5.6 m d^{-1}. Hydraulic gradient ranges from 0.001 to 0.1, with an average of $(4.2 \pm 2.5) \times 10^{-3}$. The aquifer thickness ranges from 8.7 to 77.1 m, with an average of 47.2 ± 22.1 m. The square root of the ratio of vertical hydraulic conductivity to horizontal hydraulic conductivity is assumed to be 0.6 from previous studies on Hainan

Table 1
Parameters and Estimated Values Used in Radium Mass Balance Model, Darcy Estimates, and Watershed Recharge Estimate

Parameters	Values	Description and units
Constants, estimated parameters, and field data		
D_{dis}	2×10^{-9}	Radium dispersion coefficient in water of marine sediments (Luo & Jiao, 2016) ($m^2\ s^{-1}$)
D_{mix}	6×10^{-10}	Radium mixing coefficient in water of marine sediments (Luo & Jiao, 2016) ($m^2\ s^{-1}$)
Φ	0.41	Sediment porosity in marine sediments
λ_{223}	0.061	Decay constant of ^{223}Ra (d^{-1})
λ_{228}	3.27×10^{-4}	Decay constant of ^{228}Ra (d^{-1})
S	9×10^{10}	Surface area of eastern Hainan shelf above 35 m bathymetry (m^2)
F_{SPM}	0.113	SPM deposit rate in the eastern Hainan shelf (J. Liu et al., 2014) ($g\ m^2\ d^{-1}$)
$v_{EK\text{-}T}$	0.14	Ekman transport rate in the eastern Hainan shelf (Wang et al., 2013) (Sv)
$v_{EK\text{-}P}$	0.07	Ekman pumping rate in the eastern Hainan shelf (Wang et al., 2013) (Sv)
L_c	300	The length of eastern Hainan coastal line (km)
V_s	1.58×10^{12}	Water volume of upper mixing layer above the Ekman depth of 35 m (m^3)
α_D	2.0	^{226}Ra and ^{228}Ra desorption rate from SPM (Moore, 1996; Moore et al., 2008) ($dpm\ g^{-1}$)
V_r	2.06×10^7	Total five river discharge to the eastern Hainan shelf (Li et al., 2014) ($m^3\ d^{-1}$)
$^{228}k_{ad}$	61.1 (20.5–74.2)	Adsorption coefficient of ^{228}Ra in water/sediment bulk
D_{EK}	35	Ekman depth in the eastern Hainan shelf based on field data
P_{228}	106 (39–141)	Production rate of ^{228}Ra in the sediments (dpm L^{-1} sediment)
$(^{223}Ra/^{228}Ra)_{GW}$	0.051 (0.009–0.117)	ARs of ^{223}Ra to ^{228}Ra in groundwater end-member
$(ex^{223}Ra/ex^{228}Ra)_{SW}$	0.019 (0.005–0.037)	Ratios of excess ^{223}Ra to excess ^{228}Ra in the inner shelf waters
$(^{223}Ra/^{228}Ra)_{Sub}$	0.0161	ARs of ^{223}Ra to ^{228}Ra in subsurface water of the inner shelf
$(^{223}Ra/^{228}Ra)_{EK}$	0.010 (0.008–0.012)	ARs of ^{223}Ra to ^{228}Ra in the upwelling zonal area
T_w	16.9 ± 8.9(5.4–38.2)	Water residence time in the eastern continental shelf areas (days)
T_u	10.2 ± 3.0 (5.7–14.8)	Water residence time in the upwelling zonal area (days)
λ_{mix}	0.059 (0.026–0.185)	Tidal mixing rate, reciprocal of inner shelf water residence time (d^{-1})
$^{228}Ra_{open}$	6.6 ± 0.6	^{228}Ra activity in the open seawater (dpm 100 L^{-1})
$^{226}Ra_{open}$	5.9 ± 1.1	^{226}Ra activity in the open seawater (dpm 100 L^{-1})
$^{223}Ra_{open}$	0.003 ± 0.002	^{223}Ra activity in the open seawater (dpm 100 L^{-1})
A_{226}	2545 ± 35.0	^{226}Ra activities in saline groundwater end member (dpm 100L^{-1})
A_{228}	5194 ± 217.6	^{228}Ra activities saline in groundwater end member (dpm 100L^{-1})
ΔA_{226}	1.9	^{226}Ra activity difference between inner shelf water and open sea water (dpm 100L^{-1})
ΔA_{228}	2.8	^{228}Ra activity difference between inner shelf water and open sea water (dpm 100L^{-1})
^{228}Ra mass balance model		
F_{SPM}	1.0×10^{10}	^{228}Ra from atmospheric SPM desorption ($dpm\ d^{-1}$)
F_r	1.9×10^{10}	^{228}Ra input from river discharge ($dpm\ d^{-1}$)
F_U	2.2×10^{12}	^{228}Ra input from coastal upwelling ($dpm\ d^{-1}$)
F_{SGD}	7.4×10^{11}	SGD-derived ^{228}Ra loadings ($dpm\ d^{-1}$)
F_{mix}	3.1×10^{12}	^{228}Ra mixing loss ($dpm\ d^{-1}$)
F_{decay}	7.4×10^{10}	^{228}Ra loss via decay ($dpm\ d^{-1}$)
F_{sed}	6.3×10^{10}	^{228}Ra input from physical processes, bio-irrigation, bioturbation and etc. ($dpm\ d^{-1}$)
SGD_{228}	1.1×10^8	SGD based on ^{228}Ra model ($m^3\ d^{-1}$)
^{226}Ra mass balance model		
F_{SPM}	1.0×10^{10}	^{226}Ra from atmospheric SPM desorption($dpm\ d^{-1}$)
F_r	2.2×10^{10}	^{226}Ra input from river discharge ($dpm\ d^{-1}$)
F_U	1.9×10^{12}	^{226}Ra input from coastal upwelling($dpm\ d^{-1}$)
F_{SGD}	2.1×10^{11}	SGD-derived ^{226}Ra loadings($dpm\ d^{-1}$)
F_{mix}	2.1×10^{12}	^{226}Ra mixing loss ($dpm\ d^{-1}$)
F_{sed}		^{226}Ra input from physical processes, bio-irrigation, bioturbation and etc. ($dpm\ d^{-1}$)
SGD_{226}	0.8×10^8	SGD based on ^{226}Ra model ($m^3\ d^{-1}$)
Darcy estimate		
H_a	47.2 ± 22.1	The thickness of the upper aquifer system (m)
L_c	300	The length of eastern Hainan coastal line (km)
L_w	330	The maximum with of fresh groundwater seepage face across the coastline (m)
dh/dw	0.0042 ± 0.0025	Hydraulic gradient
K_h	8.9 ± 1.9	Horizontal hydraulic conductivity ($m\ d^{-1}$)
K_v	154 ± 81	Vertical hydraulic conductivity ($m\ d^{-1}$)
Q_F	3.5×10^6	Fresh SGD ($m^3\ d^{-1}$)
Watershed recharge estimate		
P	2,200	Annual rainfall of eastern Hainan Island ($mm\ yr^{-1}$)
S_E	12 s	Recharge areas of eastern Hainan Island (km^2)

Table 1. (continued)

Parameters	Values	Description and units
α_i	0.3 ± 0.11	Infiltration rate to the upper aquifer, retrieved from (Li & Lin, 1981)
$Q_{reservoir}$	5.5×10^6	Water capacity of reservoirs and channels in the eastern Hainan Island (Zhou, 2005) ($m^3\ d^{-1}$)
Q_r	2.1×10^7	River discharge to the eastern Hainan shelf (Li et al., 2014) ($m^3\ d^{-1}$)
$Q_{extract}$	2.9×10^5	Groundwater exploitation rate in eastern Hainan Island (Zhou, 2005) ($m^3\ d^{-1}$)
Q_F	4.5×10^6	Fresh SGD ($m^3\ d^{-1}$)

Island (Li et al., 2010). The maximum width of fresh groundwater seepage face is calculated to be 330 m. This value is rather consistent with the results obtained in other coastlines of island and continental shelf systems (Kim et al., 2003; Santos et al., 2009a; Taniguchi et al., 2003, 2006). Subtitling all the parameters to equation (6), the fresh SGD is estimated to be $3.5 \times 10^6\ m^3\ d^{-1}$. The fresh SGD obtained with Darcy's law accounts for about 3.3% and 16.8% of total SGD and river discharge to the shelf system.

Fresh SGD is further estimated with watershed recharge approach as shown in equation (8). The parameters used in the watershed recharge estimate are summarized in Table 1. The precipitation of the eastern Hainan Island is 2,200 mm yr^{-1}, and the five main catchments have a total area of $\approx 13 \times 10^3\ km^2$. The infiltration coefficients, which are retrieved from 1: 50,000 and 1: 2,000,000 regional hydrogeological map sheets as described above, range from 0.1 to 0.6, with an average of 0.3 ± 0.11. The river discharge of the five main rivers emptying into the eastern Hainan shelf is $2.1 \times 10^7\ m^3\ yr^{-1}$ (Li et al., 2014; Liu et al., 2011). The groundwater exploitation of the eastern Hainan Island is $1.1 \times 10^8\ m^3\ yr^{-1}$ or $2.9 \times 10^5\ m^3\ d^{-1}$ (Zhou, 2005). The fresh SGD based on the watershed recharge approach is finally estimated to be $4.5 \times 10^6\ m^3\ d^{-1}$. The fresh SGD obtained with watershed recharge estimate accounts for about 4.1% and 21.6% of total SGD and river discharge to the shelf system. This result is well in line with the fresh SGD obtained by Darcy's law, suggesting good cross validation of the estimate. Fresh SGD obtained with Darcy's law and watershed recharge approach is about 12.1 and 15.3 times of the groundwater exploitation rate in the eastern Hainan Island. As summarized in Table 2, the percentages of fresh SGD to total SGD have wide ranges of 0.02% to

Table 2

Percentages of Fresh SGD in This Study, Compared to Parentage of Fresh SGD Estimates by Different Approaches in Coasts Elsewhere

Sites	Site descriptions	Fresh SGD Percentage	Approaches	References
Eastern Hainan shelf, China	Sand and muddy sands	3.3%	Darcy estimate/radium models[a]	This study
Eastern Hainan shelf, China	Sand and muddy sands	4.1%	Water recharge estimate/radium models	This study
Laizhou Bay, China	Mud and muddy sands	8–10%	Water and salt budgets/radium models	Wang et al. (2015b)
Tolo Harbor, China	Sand, silt and clay	<35%	Salt budget/radium models	Luo et al. (2014)
Tolo Harbor, China	Sand, silt, and clay	≈ 0.03%	Watershed recharge/radium model	Lee et al. (2012)
Lynch Cove, USA	Well sorted sands	≈ 20%	Radium model/Seepage meter & ^{222}Rn model	Swarzenski et al. (2007)
Nizanim area, Israel	Karst and sandy aquifer	38–49	Numerical modeling	Prieto and Destouni (2005)
Jesu Island, Korea	Permeable volcanic rocks	≈ 20%	Watershed recharge/seepage meter	Kim et al. (2003)
Kona coast, HI, USA	Volcanic fluvial deposit	7–67%	Salt budget/radium models	Knee et al. (2010)
Kahana Bay, HI, USA	Volcanic fluvial deposit	<20%	Salinity mixing model	Garrison et al. (2003)
Waquoit Bay, USA	Gravels and sands	<80%	Darcy estimate/^{222}Rn models	Mulligan and Charette (2006)
Waquoit Bay, USA	Gravels and sands	<23%	Spatial distribution with seepages meter	Michael et al. (2003)
Huntington beach, USA	Sandy and wavy coasts	<26%	Analytical solutions/Radium models	Boehm et al. (2006)
FSUCML, FL, USA	Coastal plain sands	2–12%	Salinity mixing model	Santos et al. (2009a)
FSUCML, FL, USA	Coastal plain sands	<16%	Freshening of seepage meter water/^{222}Rn model	Santos et al. (2009a)
FSUCML, FL, USA	Coastal plain sands	≈ 1%	Water table rate decay/^{222}Rn model	Santos et al. (2009a)
FSUCML, FL, USA	Coastal plain sands	≈ 4%	Darcy estimate/^{222}Rn model	Santos et al. (2009a)
Yellow River delta, China	Flat mud	0.4–26.9%	Salt budget/seepage meter	Taniguchi et al. (2008)
Yatsushiro Sea coasts, Japan	Volcanic rocks	6.1–37.7%	Solute budget/seepage meter	Taniguchi et al. (2006)
Tampa Bay, USA	Sand, silts, and clays	22–52%	Darcy estimate/^{222}Rn model	Kroeger et al. (2007)
Osaka Bay, Japan	Muddy sand sediment	4–29%	Darcy estimate/seepage estimate	Taniguchi and Iwakawa (2004)
South Atlantic Bight, USA	Permeable relict sands	<4%	Watershed recharge/radium model	Younger (1996); Moore (1996)
South Atlantic Bight, USA	Permeable relict sands	<4%	Analytical solutions	Li et al. (1999)

[a] Denotes "fresh SGD estimate approach/total SGD estimate approach."

over 80%. The percentages of fresh groundwater component in this study are in the low range of that obtained in previous studies. The large variability of the fresh SGD percentages would be mainly due to difference of hydrological settings of the coastal aquifer systems and the different approaches adopted (Table 2).

4.4. The Conceptual Model of Nutrient Dynamics and New Productions

The exogenous N loadings to the continental shelf will support the new production regionally. There is a paradox that the nitrogen (mostly DIN) needed to support the current observations of new productions in the mixing layer of tropic oceans are much larger than the examined exogenous N loadings (Lin et al., 2003; McGillicuddy et al., 1998, 2007). To explain the missing nitrogen to support new production in the trophic surface seawater, oceanographers have investigated the exogenous DIN loadings of different sources such as typhoon-induced injection (Lin et al., 2003; Shang et al., 2008; Siswanto et al., 2007; Son et al., 2006), internal wave-induced inputs (Chen et al., 2016; Lee Chen, 2005), mesoscale eddy-induced input (McGillicuddy et al., 1998, 2007), N_2 fixation by Trichodesmium (Wu et al., 2003; Zhang et al., 2015), and fluvial-induced loadings (Liu et al., 2012). However, there are quite limited studies to evaluate the new production supported by the shelf-scale SGD-derived nutrients loadings, which could be significant due to large magnitude of SGD over the continental shelf and high nutrient concentrations in the groundwater (Q. Liu et al., 2014; Moore et al., 2008; Rodellas et al., 2015). Thus, an important goal of this study is to evaluate the new production that supported by SGD-derived nutrient loadings.

The nutrient dynamics within the eastern Hainan shelf upwelling system is shown in the schematic of Figure 11b. The dominant partition of SGD in the study area is recirculated seawater driven by multiple forces such as tide and wave pumping at the nearshore area and convection-induced pore water exchange by salt wedge pump over the seabed of continental shelf (Gonneea & Charette, 2014; Moore & Wilson, 2005; Santos et al., 2012a). New production is defined as primary production in the euphotic zone supported by the exogenous nutrients. For the SGD in this study, the dominant component is recirculated seawater. A simple approach is employed to quantify the net DIN loadings derived from recirculated seawater as described by Santos et al. (2012a). Briefly, the net nutrient loadings derived from recirculated seawater are obtained by multiplying seawater recirculating rate with the difference between nutrient concentrations in groundwater of eastern Hainan coast and those in the bottom seawater of eastern Hainan shelf. As the nutrient concentrations in groundwater of eastern Hainan coasts are highly variable due to heterogeneity of coastal aquifers, the median values of 320 and 6.6 μM (supporting information Table S1) were used to represent DIN and DIP concentrations in groundwater end-member. The bottom seawater has less variable DIN and DIP concentrations, with an average of 20 and 0.9 μM, respectively. Thus, the net DIN and DIP loading delivered by recirculated seawater is estimated to 3.2×10^7 mol d^{-1} (or 1121.8 μM m^{-2} d^{-1}) and 5.9×10^5 mol d^{-1} (or 20.4 μM m^{-2} d^{-1}), respectively. Due to the complicated reaction processes occurring within costal groundwater mixing zones and limited nutrient information in the saline groundwater (10–30 psu), the estimation of net DIN and DIP loadings would represent the upper limit of groundwater-borne nutrients to the study area. Thus, the primary production supported by groundwater-borne DIN loadings in this study might represent the maximum estimate. Considering the phytoplankton consumes the nutrients under a stoichiometry of C: N: P = 106: 16: 1, the groundwater-induced DIN supports a maximum new production of 7.5 mM C m^2 d^{-1}. Based on the field data of nutrients, the average of DIN and DIP below the Ekman depth is calculated to be 6.5 and 0.5 μM within the Rossby radius of 55 km, and to be 7.4 and 0.6 μM within the maximum Ekman pumping occurrence radius of 150 km (Figure 11b). The coastal upwelling-induced DIN and DIP loadings are calculated to be ~2,741 and ~ 217.7 μM N m^2 d^{-1}, respectively. The coastal upwelling derived DIN loading supports a new production of 18.2 mM C m^2 d^{-1}. Further comparisons are made between groundwater-borne DIN supported new production and that supported by other exogenous DIN loadings in the eastern Hainan shelf as shown in Figure 11. Based on the time series studies by remote sensing approaches, Kim et al. (2014) estimated an atmospheric deposit of ~150.7 μM N m^2 d^{-1}, which supported new production of ~1 mM C m^2 d^{-1}. Zhang et al. (2015) investigated the N_2 fixation of eastern Hainan shelf to be ≈ 46.4 μM N m^2 d^{-1}, and the new production supported by N_2 fixation is calculated to be 0.3 mM C m^2 d^{-1}. The riverine derived DIN loadings to the eastern Hainan shelf is estimated to be 5.9 μM N m^2 d^{-1}, and the supported new production is 40 μM C m^2 d^{-1}. The diffusion loading of DIN driven by the vertical DIN gradient is estimated to be 604 μM N m^2 d^{-1}, based on an one dimensional ^{228}Ra diffusion model (Cai et al., 2002), and DIN supported by this process supports a new production of 4.4 mM C m^2 d^{-1}. As there is no typhoon and mesoscale eddy developed during the sampling period, DIN loadings from

Table 3

New Productions Supported by Different DIN Sources and its Comparison With Previous Studies

Parameters	Values	Description and units
$[DIN]_{Rossb}$	6.5	DIN concentration in the Rossby radius below Ekman depth (μM)
$[DIN]_{150km}$	7.4	DIN concentration in from the pixel of transport pumping below Ekman depth (μM)
$[DIP]_{Rossby}$	0.51	DIP concentration in the Rossby radius below Ekman depth (μM)
$[DIP]_{150km}$	0.6	DIN concentration in from the pixel of transport pumping below Ekman depth (μM)
Exogenous DIN loadings for new production	5.9	Total riverine derived DIN loadings (μM m^2 d^{-1})
	150.7	Atmospheric deposit DIN loadings (μM m^2 d^{-1})
	46.4	N_2 fixation rate (μM m^2 d^{-1})
	2741.8	Upwelling derived DIN loadings to the mixing layer (μM m^2 d^{-1})
	603.8	Diffusion input derived from DIN gradients in water column (μM m^2 d^{-1})
	$\leq$1121.8	SGD-derived DIN loadings (μM m^2 d^{-1})
Exogenous DIP loadings for new production	2.1	Total riverine derived DIP loadings (μM m^2 d^{-1})
		Atmospheric deposit DIN loadings (μM m^2 d^{-1})
		N_2 fixation rate (μM m^2 d^{-1})
	217.7	Upwelling derived DIP loadings to the mixing layer (μM m^2 d^{-1})
	$\leq$ 20.4	SGD-derived DIP loadings (μM m^2 d^{-1})
New production supported by exogenous DIN	0.04	Riverine-derived DIN supported new production (mM C m^{-2} d^{-1})
	$\approx$ 1	Atmospheric deposit DIN supported new production (μM C m^{-2} d^{-1}) (Kim et al., 2014)
	18.2	Coastal upwelling DIN supported new production (mM C m^{-2} d^{-1})
	$\leq$ 7.5	SGD-derived DIN supported new production (mM C m^{-2} d^{-1})
	0.3	N_2 fixation supported new productions (mM C m^{-2} d^{-1}) (Zhang et al., 2015)
	4.4	New productions derived from diffusion input (mM C m^{-2} d^{-1}) (Cai et al., 2002)
	31.3	Total new productions in the eastern china sea (mM C m^{-2} d^{-1})
New productions in previous studies at the adjacent seas		
Chen et al. (2004)	5–30	NSCS close to Luzon Strait (mM C m^{-2} d^{-1})
Lee Chen (2005)	2.5–21.7	NSCS from shelf to basin (mM C m^{-2} d^{-1})
Lee Chen and Chen (2006)	10–20.8	NSCS closed to Taiwan Strait and Luzon Strait (mM C m^{-2} d^{-1})
Chen et al. (2007)	20.8–55.8	Cold eddy areas at NSCS, Luzon Strait, and West Philippine Sea (mM C m^{-2} d^{-1})
Wong et al. (2007)	4.2–8.3	South East Asian Tune-series Study (SEATS) station in NSCS (mM C m^{-2} d^{-1})
Chen et al. (2008)	13.3–22.5	Upstream Kuroshio and SCS basin (mM C m^{-2} d^{-1})
Kim et al. (2014)	4.2–6.7	The whole SCS (mM C m^{-2} d^{-1})
Wong et al. (2015)	27.5 $\pm$ 17.5	NSCS (mM C m^{-2} d^{-1})
Zhang et al. (2015)	12.5–52.5	Southeastern Hainan shelf (mM C m^{-2} d^{-1})

these processes are therefore negligible. Thus, total new production in the eastern Hainan shelf is summed up to be 31.3 mM C m^2 d^{-1}. New production supported by groundwater-borne DIN constitutes about up to 24.0% of the total new production, suggesting that groundwater-borne nutrients could be an important exogenous DIN source for new productions in the mixing layer of trophic oceans. Further comparisons are made between the new productions obtained in eastern Hainan shelf with other adjacent seas in SCS, as shown in Table 3. The obtained new production in the eastern Hainan shelf is relatively higher than but still falls within the ranges of new productions observed in the adjacent seas in SCS. The SGD-derived nutrient loadings may well explain the missing DIN that supports the new productions in this tropic oligotrophic ocean.

4.5. Uncertainty Analysis

The cumulative ^{226}Ra and ^{228}Ra inputs from river discharge, sedimentary processes, and atmospheric deposit to the eastern Hainan shelf are relatively small, in total representing less than 5% and 6% in the ^{226}Ra and ^{228}Ra mass balance models, respectively (Table 1). Thus, under steady state, the SGD-derived radium inputs are mainly balanced by the major sink of oceanic mixing. In this study, the mixing loss is calculated based on the $^{226/228}$Ra excesses and the average water residence time calculated with equations (1) and (2). Therefore, the uncertainties in the SGD estimate mainly stem from the variability of water residence time, the uncertainties of ^{226}Ra and ^{228}Ra excess estimates, and the variation of radium activities in groundwater end-member, as suggested in other similar SGD studies (Gonneea et al., 2013; Liu et al., 2012, Q. Liu et al., 2014; Rodellas et al., 2017). The uncertainties in estimates of ^{226}Ra and ^{228}Ra excesses are mainly from the measurement error and have ranges of 15–20% and 7–12%, respectively (Q. Liu et al., 2014). The variation of 1 day will induce a change of 4–6% of the final SGD estimate. The water residence time is estimated to be 16.9 ± 8.9 days, which will lead to large uncertainties of 36–54% in the final SGD estimate. However, the uncertainties in the water residence time estimates in the continental shelf are inevitable and natural, as water ages are expected to vary with distance from the coastlines (Q. Liu et al., 2014; Moore, 2000). The uncertainties of ^{226}Ra and ^{228}Ra in groundwater end-members are estimated to be 14% and 42% in saline groundwater, respectively. This variability in groundwater end-member is due to the spatial heterogeneity of aquifer system and temporal variability of coastal hydrodynamic conditions (Cho & Kim, 2016; Gonneea et al., 2013). For the above reasons, it is mostly likely that the uncertainties based on ^{226}Ra and ^{228}Ra would be of the same order of magnitude to that of the final SGD estimates. But placing an exact value on the uncertainties of radium mass balance models in this study would still be a challenging task (Gonneea et al., 2013; Q. Liu et al., 2014) and further studies are required to refine the uncertainties involved in the radium-based SGD estimate (Santos et al., 2009a; Wang et al., 2015b). Even due to large uncertainties, however, the obtained total SGD and the related uncertainties are well in line with those obtained in other SGD studies of continental shelf systems (Gonneea et al., 2013; Liu et al., 2012, Q. Liu et al., 2014; Moore, 2007; Rodellas et al., 2017), giving the confidence of results in this study. For the estimates of SGD-derived net DIN and DIP loadings, the uncertainties might stem from the lack of nutrient data in the saline groundwater (10–30 psu) or recirculated seawater, Due to relatively complicated processes occurring in the saline groundwater, nutrient loading delivered by the recirculated seawater may not always represent the new or exogenous nutrient loadings. Thus, the estimate of new production supported by groundwater-borne DIN in this study would account for the upper limit.

5. Conclusions

To conclude, this study examines the hydrographic dynamics in the eastern Hainan shelf based on cruise observational data. The shelf system is characterized by coastal upwelling, which delivers large radium isotopes and nutrients to the upper mixing layer. Based on the investigation of radium distribution, a radium mixing model is used to quantify water residence time, leading to an estimate of 5.4–38.2 days, with an average of 16.9 ± 8.9 days for the study area. Coastal upwelling coupled radium mass balance models are established to quantify the SGD in the system. The total SGD is estimated to be $(0.8–1.4) \times 10^8$ m^3 d^{-1}. Furtherly, based on Darcy's Law and watershed recharge approach, fresh SGD is obtained to be 3.5×10^6 and 4.5×10^6 m^3 d^{-1}, respectively. The fresh SGD contributes about 3.3–4.1% of the total SGD. The SGD-derived nutrient loadings to the shelf system in the summer time are estimated to be 1,121.8 and 20.1 μM m^2 d^{-1}, for DIN and DIP, respectively. DIN and DIP loadings by coastal upwelling is estimated to be 2,741.6 and 217.7 μM m^2 d^{-1}, respectively. The results reveal that groundwater-borne nutrients will be comparable to the nutrients loadings by coastal upwelling. The new production supported by the coastal upwelling is estimated to be 18.2 mM C m^2 d^{-1}, which comprised of 58.1% of the total new production in HEU. Groundwater-borne nutrients will support a maximum new production of 7.5 mM C m^2 d^{-1}, which contributes up to 25.6% of the total new production in HEU. New productions supported by groundwater-borne nutrients and coastal upwelling are predominant compared to that supported by other exogenous N loadings such as atmospheric deposit and fluvial loadings. The surface water of eastern Hainan shelf is oligotrophic located within the trophic areas and is featured by relatively high primary production and new production. This study provides a new prospective to examine the missing N that is required to support the observed new productions in the trophic ocean surface water and can be instructive to the biogeochemical studies in other upwelling systems in the tropic oligotrophic oceans.

Acknowledgments

This study was supported by a grant from National Natural Science Foundation of China (41372261) and the Research Grants Council of Hong Kong (HKU 7028/06P). The remote sensing data of SST and SSChla are sourced from MODIS-Aqua from https://oceancolor.gsfc.nasa.gov/data/aqua/#. The data of surface of velocity fields are sourced from OSCAR from http://coastwatch.pfeg.noaa.gov/erddap/griddap/jplOscar.html. The high-resolution CTD data (1 m) are sourced from Wang Dongxiao and can be obtained from L. X. (email: xinluo@hku.hk). Other data reported in the study are listed in the *Data set 1*. Appreciations are given to Eddie Ho, Maple Kwong, Alan Kowk, Mike Chio, and Ergang Lian for their kind help in the cruise preparation, sample analysis, and data interpretations. Thanks are given to Liang Dong from Tongji University, and Ziming Fang from Xiamen University for their help of sampling on board. The authors thank Mario Lo and Jessie Lai for their help of nutrient analysis with Flow Injection Analysis in the school of biological sciences. The authors thank Billy Moore for his help in radium analysis. The authors owe thanks to the crew of *R/V Shiyan III* for their help during the cruises. The authors owe thanks to the editor Prof. S. Bradley Moran and the anonymous reviewers for their constructive comments which greatly improved the manuscript.

References

Allen, J. S. (1973). Upwelling and coastal jets in a continuously stratified ocean. *Journal of Physical Oceanography*, *3*(3), 245–257.

Bakun, A., & Nelson, C. S. (1991). The seasonal cycle of wind-stress curl in subtropical eastern boundary current regions. *Journal of Physical Oceanography*, *21*(12), 1815–1834.

Blanco, A. C., Watanabe, A., Nadaoka, K., Motooka, S., Herrera, E. C., & Yamamoto, T. (2011). Estimation of nearshore groundwater discharge and its potential effects on a fringing coral reef. *Marine Pollution Bulletin*, *62*(4), 770–785. https://doi.org/10.1016/J.Marpolbul.2011.01.005

Boehm, A. B., Paytan, A., Shellenbarger, G. G., & Davis, K. A. (2006). Composition and flux of groundwater from a California beach aquifer: Implications for nutrient supply to the surf zone. *Continental Shelf Research*, *26*(2), 269–282.

Bokuniewicz, H. J. (1992). Analytical descriptions of subaqueous groundwater seepage. *Estuaries*, *15*(4), 458–464. https://doi.org/10.2307/1352390

Bratton, J. F. (2010). The three scales of submarine groundwater flow and discharge across passive continental margins. *Journal of Geology*, *118*(5), 565–575 https://doi.org/10.1086/655114

Burnett, W. C., Bokuniewicz, H., Huettel, M., Moore, W. S., & Taniguchi, M. (2003). Groundwater and pore water inputs to the coastal zone. *Biogeochemistry*, *66*(1–2), 3–33.

Burt, W. J., Thomas, H., Pätsch, J., Omar, A., Schrum, C., Daewel, U., . . . Baar, H. (2014). Radium isotopes as a tracer of sediment-water column exchange in the North Sea. *Global Biogeochemistry Cycles*, *28*, 786–804. https://doi.org/10.1002/2014GB004825

Cai, P., Huang, Y. P., Chen, M., Guo, L. D., Liu, G. S., & Qiu, Y. S. (2002). New production based on Ra-228-derived nutrient budgets and thorium-estimated POC export at the intercalibration station in the South China Sea. *Deep Sea Res Part I: Oceanographic Research Papers*, *49*(1), 53–66.

Cai, P., Shi, X., Hong, Q., Li, Q., Liu, L., Guo, X., & Dai, M. (2015). Using ^{224}Ra/^{228}Th disequilibrium to quantify benthic fluxes of dissolved inorganic carbon and nutrients into the Pearl River Estuary. *Geochimica et Cosmochimica Acta*, *170*, 188–203.

Cambareri, T. C., & Eichner, E. M. (1998). Watershed delineation and ground water discharge to a coastal embayment. *Ground Water*, *36*(4), 626–634.

Cao, Z., Dai, M., Zheng, N., Wang, D., Li, Q., Zhai, W., . . . Gan, J. (2011). Dynamics of the carbonate system in a large continental shelf system under the influence of both a river plume and coastal upwelling. *Journal of Geophysical Research: Biogeosciences*, *116*, G02010. https://doi.org/10.1029/2010JG001596

Charette, M. A., Buesseler, K. O., & Andrews, J. E. (2001). Utility of radium isotopes for evaluating the input and transport of groundwater-derived nitrogen to a Cape Cod estuary. *Limnology and Oceanography*, *46*(2), 465–470.

Charette, M. A., Morris, P. J., Henderson, P. B., & Moore, W. S. (2015). Radium isotope distributions during the US GEOTRACES North Atlantic cruises. *Marine Chemistry*, *177*, 184–195.

Chavez, F. P., Barber, R., & Sanderson, M. (1989). *Potential primary production of the Peruvian upwelling ecosystem, 1953–1984*. In *The Peruvian upwelling ecosystem: Dynamics and interactions* (Vol. 18, 50 pp.). Penang, Malaysia: WorldFish.

Chavez, F. P., & Toggweiler, J. (1994 September 25–30). Physical estimates of global new production: The up-welling contribution. In *Dahlem workshop on upwelling in the ocean: Modern processes and ancient records* (pp. 313–320). Chichester, UK: John Wiley.

Chavez, F. P., & Messié, M. (2009). A comparison of eastern boundary upwelling ecosystems. *Progress in Oceanography*, *83*(1–4), 80–96. https://doi.org/10.1016/j.pocean.2009.07.032

Chelton, D. B., Deszoeke, R. A., Schlax, M. G., El Naggar, K., & Siwertz, N. (1998). Geographical variability of the first baroclinic Rossby radius of deformation. *Journal of Physical Oceanography*, *28*(3), 433–460.

Chen, T. Y., Tai, J. H., Ko, C. Y., Hsieh, C. H., Chen, C. C., Jiao, N., . . . Shiah, F. K. (2016). Nutrient pulses driven by internal solitary waves enhance heterotrophic bacterial growth in the South China Sea. *Environmental Microbiology*, *18*(12), 4312–4323.

Chen, W. F., Liu, Q. A., Huh, C. A., Dai, M. H., & Miao, Y. C. (2010). Signature of the Mekong River plume in the western South China Sea revealed by radium isotopes. *Journal of Geophysical Research: Oceans*, *115*, C12002. https://doi.org/10.1029/2010JC006460

Chen, Y.-L. L., Chen, H.-Y., Karl, D. M., & Takahashi, M. (2004). Nitrogen modulates phytoplankton growth in spring in the South China Sea. *Continental Shelf Research*, *24*(4), 527–541.

Chen, Y.-L. L., Chen, H.-Y., Lin, I.-I., Lee, M.-A., & Chang, J. (2007). Effects of cold eddy on phytoplankton production and assemblages in Luzon Strait bordering the South China Sea. *Journal of Oceanography*, *63*(4), 671–683.

Chen, Y-L. L., Chen, H.-Y., Tuo, S-h., & Ohki, K. (2008). Seasonal dynamics of new production from Trichodesmium N_2 fixation and nitrate uptake in the upstream Kuroshio and South China Sea basin. *Limnology and Oceanography*, *53*(5), 1705–1721.

Cho, H. M., & Kim, G. (2016). Determining groundwater Ra end-member values for the estimation of the magnitude of submarine groundwater discharge using Ra isotope tracers. *Geophysical Research Letters*, *43*(8), 3865–3871.

Chi, P. C., Chen, Y., & Lu, S. (1998). Wind-driven South China Sea deep basin warm-core/cool-core eddies. *Journal of Oceanography*, *54*(4), 347–360.

D'Andrea, A. F., Lopez, G. R., & Aller, R. C. (2004). Rapid physical and biological particle mixing on an intertidal sandflat. *Journal of Marine Research*, *62*(1), 67–92.

De Sieyes, N. R., Yamahara, K. M., Layton, B. A., Joyce, E. H., & Boehm, A. B. (2008). Submarine discharge of nutrient-enriched fresh groundwater at Stinson Beach, California is enhanced during neap tides. *Limnology and Oceanography*, *53*(4), 1434–1445.

Dugdale, R., & Goering, J. (1967). Uptake of new and regenerated forms of nitrogen in primary productivity. *Limnology and Oceanography*, *12*(2), 196–206.

Dugdale, R., Wilkerson, F., & Morel, A. (1990). Realization of new production in coastal upwelling areas: A means to compare relative performance. *Limnology and Oceanography*, *35*(4), 822–829.

Encarnação, J., Leitão, F., Range, P., Piló, D., Chícharo, M. A., & Chícharo, L. (2013). The influence of submarine groundwater discharges on subtidal meiofauna assemblages in south Portugal (Algarve). *Estuarine, Coastal and Shelf Science*, *130*, 202–208.

Fang, W., Fang, G., Shi, P., Huang, Q., & Xie, Q. (2002). Seasonal structures of upper layer circulation in the southern South China Sea from in situ observations. *Journal of Geophysical Research: Oceans*, *107*(C11).

Fetter, C. W., & Fetter, C. (2001). *Applied hydrogeology*. Upper Saddle River, NJ: Prentice Hall.

Garrison, G., Glenn, C., & McMurtry, G. (2003). Measurement of submarine groundwater discharge in Kahana Bay, O'ahu, Hawaii. *Limnology and Oceanography*, *48*(2), 920–928.

Gattuso, J. P., Frankignoulle, M., & Wollast, R. (1998). Carbon and carbonate metabolism in coastal aquatic ecosystems. *Annual Review of Ecology and Systematics*, *29*, 405–434.

Gonneea, M. E., & Charette, M. A. (2014). Hydrologic controls on nutrient cycling in an unconfined coastal aquifer. *Environmental Science & Technology*, *48*(24), 14178–14185.

Gonneea, M. E., Mulligan, A. E., & Charette, M. A. (2013). Seasonal cycles in radium and barium within a subterranean estuary: Implications for groundwater derived chemical fluxes to surface waters. *Geochimica et Cosmochimica*, *119*, 164–177.

Green, M., Aller, R., Cochran, J., Lee, C., & Aller, J. (2002). Bioturbation in shelf/slope sediments off Cape Hatteras, North Carolina: The use of ^{234}Th, Chl-a, and Br− to evaluate rates of particle and solute transport. *Deep Sea Research Part II: Topical Studies in Oceanography*, *49*(20), 4627–4644.

Han, A., Dai, M., Gan, J., Kao, S.-J., Zhao, X., Jan, S., . . . Wang, L. (2013). Inter-shelf nutrient transport from the East China Sea as a major nutrient source supporting winter primary production on the northeast South China Sea shelf. *Biogeosciences*, *10*(12), 8159–8170.

Hancock, G. J., Webster, I. T., & Stieglitz, T. C. (2006). Horizontal mixing of Great Barrier Reef waters: Offshore diffusivity determined from radium isotope distribution. *Journal of Geophysical Research: Oceans*, *111*, C12019. https://doi.org/10.1029/2006JC003608

Hedges, J. I. (1992). Global biogeochemical cycles: Progress and problems. *Marine Chemistry*, *39*(1–3), 67–93. https://doi.org/10.1016/0304-4203(92)90096-S

Hu, J., Kawamura, H., Hong, H., & Qi, Y. (2000). A review on the currents in the South China Sea: seasonal circulation, South China Sea warm current and Kuroshio intrusion. *Journal of Oceanography*, *56*(6), 607–624.

Hu, J., & Wang, X. H. (2016). Progress on upwelling studies in the China seas. *Reviews of Geophysics*, *54*, 653–673. https://doi.org/10.1002/2015RG000505

Huettel, M., Ziebis, W., Forster, S., & Luther, G. (1998). Advective transport affecting metal and nutrient distributions and interfacial fluxes in permeable sediments. *Geochimica et Cosmochimica Acta*, *62*(4), 613–631.

Jahnke, R. A., Nelson, J. R., Marinelli, R. L., & Eckman, J. E. (2000). Benthic flux of biogenic elements on the Southeastern US continental shelf: Influence of pore water advective transport and benthic microalgae. *Continental Shelf Research*, *20*(1), 109–127.

Ji, T., Du, J., Moore, W. S., Zhang, G., Su, N., & Zhang, J. (2012). Nutrient inputs to a Lagoon through submarine groundwater discharge: The case of Laoye Lagoon, Hainan, China. *Journal of Marine Systems*, *111*, 253–262.

Jing, Z., Qi, Y., & Du, Y. (2011). Upwelling in the continental shelf of northern South China Sea associated with 1997–1998 El Niño. *Journal of Geophysical Research: Oceans*, *116*, C02033. https://doi.org/10.1029/2010JC006598

Jing, Z., Qi, Y., Du, Y., Zhang, S., & Xie, L. (2015). Summer upwelling and thermal fronts in the northwestern South China Sea: Observational analysis of two mesoscale mapping surveys. *Journal of Geophysical Research: Oceans*, *120*, 1993–2006. https://doi.org/10.1002/2014JC010601

Jing, Z.-y., Qi, Y-Q., Hua, Z-L., & Zhang, H. (2009). Numerical study on the summer upwelling system in the northern continental shelf of the South China Sea. *Continental Shelf Research*, *29*(2), 467–478.

Johannes, R. E., & Hearn, C. J. (1985). The effect of submarine groundwater discharge on nutrient and salinity regimes in a coastal lagoon off Perth, Western-Australia. *Estuarine Coastal and Shelf Science*, *21*(6), 789–800.

Kim, G., Burnett, W. C., Dulaiova, H., Swarzenski, P. W., & Moore, W. S. (2001). Measurement of Ra-224 and Ra-226 activities in natural waters using a radon-in-air monitor. *Environmental Science & Technology*, *35*(23), 4680–4683.

Kim, G., Lee, K. K., Park, K. S., Hwang, D. W., & Yang, H. S. (2003). Large submarine groundwater discharge (SGD) from a volcanic island. *Geophysical Research Letters*, *30*(21), 2098. https://doi.org/10.1029/2003gl018378

Kim, G., Ryu, J. W., Yang, H. S., & Yun, S. T. (2005). Submarine groundwater discharge (SGD) into the Yellow Sea revealed by Ra-228 and Ra-226 isotopes: Implications for global silicate fluxes. *Earth and Planetary Science Letters*, *237*(1–2), 156–166. https://doi.org/10.1016/j.epsl.2005.06.011

Kim, T. W., Lee, K., Duce, R., & Liss, P. (2014). Impact of atmospheric nitrogen deposition on phytoplankton productivity in the South China Sea. *Geophysical Research Letters*, *41*, 3156–3162. https://doi.org/10.1002/2014GL059665

Knee, K. L., Street, J. H., Grossman, E. E., Boehm, A. B., & Paytan, A. (2010). Nutrient inputs to the coastal ocean from submarine groundwater discharge in a groundwater-dominated system: Relation to land use (Kona coast, Hawai'i, USA). *Limnology and Oceanography*, *55*(3), 1105.

Kotwicki, L., Grzelak, K., Czub, M., Dellwig, O., Gentz, T., Szymczycha, B., & Böttcher, M. (2014). Submarine groundwater discharge to the Baltic coastal zone: Impacts on the meiofaunal community. *Journal of Marine Systems*, *129*, 118–126.

Kroeger, K. D., Swarzenski, P. W., Greenwood, W. J., & Reich, C. (2007). Submarine groundwater discharge to Tampa Bay: Nutrient fluxes and biogeochemistry of the coastal aquifer. *Marine Chemistry*, *104*(1–2), 85–97. https://doi.org/10.1016/j.marchem.2006.10.012

Kwon, E. Y., Kim, G., Primeau, F., Moore, W. S., Cho, H. M., DeVries, T., . . . Cho, Y. K. (2014). Global estimate of submarine groundwater discharge based on an observationally constrained radium isotope model. *Geophysical Research Letters*, *41*, 8438–8444. https://doi.org/10.1002/2014GL061574

Lamontagne, S., Le Gal La Salle, C., Hancock, G. J., Webster, I. T., Simmons, C. T., Love, A. J., . . . Fallowfield, H. J. (2008). Radium and radon radioisotopes in regional groundwater, intertidal groundwater, and seawater in the Adelaide Coastal Waters Study area: Implications for the evaluation of submarine groundwater discharge. *Marine Chemistry*, *109*(3–4), 318–336. https://doi.org/10.1016/j.marchem.2007.08.010

Lamontagne, S., Taylor, A. R., Herpich, D., & Hancock, G. J. (2015). Submarine groundwater discharge from the South Australian Limestone Coast region estimated using radium and salinity. *Journal of Environmental Radioactivity*, *140*, 30–41. https://doi.org/10.1016/j.jenvrad.2014.10.013

Lee Chen, Y.-L. (2005). Spatial and seasonal variations of nitrate-based new production and primary production in the South China Sea. *Deep Sea Research Part I: Oceanographic Research Papers*, *52*(2), 319–340. https://doi.org/10.1016/j.dsr.2004.11.001

Lee Chen, Y.-L., & Chen, H.-Y. (2006). Seasonal dynamics of primary and new production in the northern South China Sea: The significance of river discharge and nutrient advection. *Deep Sea Research Part I: Oceanographic Research Papers*, *53*(6), 971–986. https://doi.org/10.1016/j.dsr.2006.02.005

Lee, C. M., Jiao, J. J., Luo, X., & Moore, W. S. (2012). Estimation of submarine groundwater discharge and associated nutrient fluxes in Tolo Harbour, Hong Kong. *The Science of the Total Environment*, *433*, 427–433. https://doi.org/10.1016/j.scitotenv.2012.06.073

Lee, H., Kim, G., Kim, J., Park, G., & Song, K. H. (2014). Tracing the flow rate and mixing ratio of the Changjiang diluted water in the northwestern Pacific marginal seas using radium isotopes. *Geophysical Research Letters*, *41*, 4637–4645. https://doi.org/10.1002/2014GL060230

Le Gland, G., Mémery, L., Aumont, O., & Resplandy, L. (2017). Improving the inverse modeling of a trace isotope: How precisely can radium-228 fluxes toward the ocean and submarine groundwater discharge be estimated? *Biogeosciences*, *14*(13), 3171–3189.

Li, F., & Lin, Y. (1981). *Hainan Province 1: 200,000 regional hydrogeological survey report* (In Chinese). Hainan Geological Brigade, Geology Bureau of Guangdong Province. National Geological Archives of China.

Li, H., Sun, P., Chen, S., Xia, Y., & Liu, S. (2010). A falling-head method for measuring intertidal sediment hydraulic conductivity. *Ground Water*, *48*(2), 206–211.

Li, L., Barry, D., Stagnitti, F., & Parlange, J. Y. (1999). Submarine groundwater discharge and associated chemical input to a coastal sea. *Water Resource Research*, *35*(11), 3253–3259.

Li, R. H., Liu, S. M., Li, Y. W., Zhang, G. L., Ren, J. L., & Zhang, J. (2014). Nutrient dynamics in tropical rivers, lagoons, and coastal ecosystems of eastern Hainan Island, South China Sea. *Biogeosciences*, *11*(2), 481–506.

Liao, X., Zhan, H., & Du, Y. (2016). Potential new production in two upwelling regions of the western Arabian Sea: Estimation and comparison. *Journal of Geophysical Research: Oceans*, *121*, 4487–4502. https://doi.org/10.1002/2016JC011707

Lin, I., Liu, W. T., Wu, C. C., Wong, G. T. F., Hu, C., Chen, Z., . . . Liu, K. K. (2003). New evidence for enhanced ocean primary production triggered by tropical cyclone. *Geophysical Research Letters*, *30*(13), 1718. https://doi.org/10.1029/2003GL017141

Lin, P., Cheng, Gan, P. J., & Hu, J. (2016a). Dynamics of wind-driven upwelling off the northeastern coast of Hainan Island. *Journal of Geophysical Research: Oceans*, *121*, 1160–1173. https://doi.org/10.1002/2015JC011000

Lin, P., Hu, J., Zheng, Q., Sun, Z., & Zhu, J. (2016b). Observation of summertime upwelling off the eastern and northeastern coasts of Hainan Island, China. *Ocean Dynamics*, *66*(3), 387–399.

Liu, G., Huang, Y., Chen, M., Qiu, Y., Cai, Y., & Gao, Z. (2001). Specific activity and distribution of natural radionuclides and ^{137}Cs in surface sediments of the northeastern South China Sea. *Acta Oceanologica Sinica*, *23*(6), 76–84.

Liu, J., Clift, P. D., Yan, W., Chen, Z., Chen, H., Xiang, R., & Wang, D. (2014). Modern transport and deposition of settling particles in the northern South China Sea: Sediment trap evidence adjacent to Xisha Trough. *Deep Sea Research Part I: Oceanographic Research Papers*, *93*, 145–155.

Liu, Q., Charette, M. A., Henderson, P. B., McCorkle, D. C., Martin, W., & Dai, M. (2014). Effect of submarine groundwater discharge on the coastal ocean inorganic carbon cycle. *Limnology and Oceanography*, *59*(5), 1529–1554.

Liu, Q., Dai, M., Chen, W., Huh, C.-A., Wang, G., Li, Q., & Charette, M. A. (2012). How significant is submarine groundwater discharge and its associated dissolved inorganic carbon in a river-dominated shelf system? *Biogeociences*, *9*(5), 1777–1795.

Liu, S. M., Li, R. H., Zhang, G. L., Wang, D. R., Du, J. Z., Herbeck, L. S., . . . Ren, J. L. (2011). The impact of anthropogenic activities on nutrient dynamics in the tropical Wenchanghe and Wenjiahoe Estuary and Lagoon system in East Hainan, China. *Marine Chemistry*, *125*(1), 49–68.

Luo, X., & Jiao, J. J. (2016). Submarine groundwater discharge and nutrient loadings in Tolo Harbor, Hong Kong using multiple geotracer-based models, and their implications of red tide outbreaks. *Water Research*, *102*, 11–31.https://doi.org/10.1016/j.watres.2016.06.017

Luo, X., Jiao, J. J., Moore, W., & Lee, C. M. (2014). Submarine groundwater discharge estimation in an urbanized embayment in Hong Kong via short-lived radium isotopes and its implication of nutrient loadings and primary production. *Marine Pollution Bulletin*, *82*(1), 144–154.

Luo, X., Jiao, J. J., Wang, X.-S., Liu, K., Lian, E., & Yang, S. (2017). Groundwater discharge and hydrologic partition of the lakes in desert environment: Insights from stable ^{18}O/^{2}H and radium isotopes. *Journal of Hydrology*, *546*, 189–203.

McGillicuddy, D. J., Anderson, L. A., Bates, N. R., Bibby, T., Buesseler, K. O., Carlson, C. A., . . . Goldthwait, S. A. (2007). Eddy/wind interactions stimulate extraordinary mid-ocean plankton blooms. *Science*, *316*(5827), 1021–1026.

McGillicuddy, D. J., Robinson, A., Siegel, D., Jannasch, H., Johnson, R., Dickey, T., . . . Knap, A. (1998). Influence of mesoscale eddies on new production in the Sargasso Sea. *Nature*, *394*(6690), 263–266.

Messié, M., & Chavez, F. P. (2015). Seasonal regulation of primary production in eastern boundary upwelling systems. *Progress in Oceanography*, *134*, 1–18.

Messié, M., Ledesma, J., Kolber, D. D., Michisaki, R. P., Foley, D. G., & Chavez, F. P. (2009). Potential new production estimates in four eastern boundary upwelling ecosystems. *Progress in Oceanography*, *83*(1–4), 151–158. https://doi.org/10.1016/j.pocean.2009.07.018

Michael, H. A., Lubetsky, J. S., & Harvey, C. F. (2003). Characterizing submarine groundwater discharge: A seepage meter study in Waquoit Bay, Massachusetts. *Geophysical Research Letters*, *30*(6), 1297, https://doi.org/10.1029/2002GL016000

Moore, W. S. (1976). Sampling radium-228 in the deep ocean. *Deep Sea Research Oceanography Abstract*, *23*, 647–651.

Moore, W. S. (1996). Large groundwater inputs to coastal waters revealed by Ra-226 enrichments. *Nature*, *380*(6575), 612–614.

Moore, W. S. (2000). Ages of continental shelf waters determined from Ra-223 and Ra-224. *Journal of Geophysical Research: Oceans*, *105*(C9), 22117–22122.

Moore, W. S. (2007). Seasonal distribution and flux of radium isotopes on the southeastern US continental shelf. *Journal of Geophysical Research: Oceans*, *112*, C10013. https://doi.org/10.1029/2007JC004199

Moore, W. S. (2010). The effect of submarine groundwater discharge on the ocean. *Annual Review of Marine Science*, *2*, 59–88. https://doi.org/10.1146/Annurev-Marine-120308-081019

Moore, W. S., Beck, M., Riedel, T., van der Loeff, M. R., Dellwig, O., Shaw, T. J., . . . Brumsack, H.-J. (2011). Radium-based pore water fluxes of silica, alkalinity, manganese, DOC, and Uranium: A decade of studies in the German Wadden Sea. *Geochimica et Cosmochimica Acta*, *75*, 6535–6555.

Moore, W. S., Blanton, J. O., & Joye, S. B. (2006). Estimates of flushing times, submarine groundwater discharge, and nutrient fluxes to Okatee Estuary, South Carolina. *Journal of Geophysical Research: Oceans*, *111*, C09006. https://doi.org/10.1029/2005JC003041

Moore, W. S., Sarmiento, J. L., & Key, R. M. (2008). Submarine groundwater discharge revealed by Ra-228 distribution in the upper Atlantic Ocean. *Nature Geoscience*, *1*(5), 309–311. https://doi.org/10.1038/ngeo183

Moore, W. S., & Wilson, A. M. (2005). Advective flow through the upper continental shelf driven by storms, buoyancy, and submarine groundwater discharge. *Earth and Planetary Science Letters*, *235*(3–4), 564–576. https://doi.org/10.1016/j.epsl.2005.04.043

Mulligan, A. E., & Charette, M. A. (2006). Intercomparison of submarine groundwater discharge estimates from a sandy unconfined aquifer. *Journal of Hydrology*, *327*(3), 411–425.

Oberdorfer, J. A. (2003). Hydrogeologic modeling of submarine groundwater discharge: Comparison to other quantitative methods. *Biogeochemistry*, *66*(1), 159–169.

Peterson, R. N., Moore, W. S., Chappel, S. L., Viso, R. F., Libes, S. M., & Peterson, L. E. (2016). A new perspective on coastal hypoxia: The role of saline groundwater. *Marine Chemistry*, *179*, 1–11. https://doi.org/10.1016/j.marchem.2015.12.005

Precht, E., & Huettel, M. (2003). Advective pore-water exchange driven by surface gravity waves and its ecological implications. *Limnology and Oceanography*, *48*(4), 1674–1684.

Prieto, C., & Destouni, G. (2005). Quantifying hydrological and tidal influences on groundwater discharges into coastal waters. *Water Resource Research*, *41*, W12427. https://doi.org/10.1029/2004WR003920

Qu, T. (2000). Upper-layer circulation in the South China Sea. *Journal of Physical Oceanography*, *30*(6), 1450–1460.

Rodellas, V., Garcia-Orellana, J., Masqué, P., Feldman, M., & Weinstein, Y. (2015). Submarine groundwater discharge as a major source of nutrients to the Mediterranean Sea. *Proceedings of the National Academy of Sciences United States of America*, *112*(13), 3926–3930. https://doi.org/10.1073/pnas.1419049112

Rodellas, V., Garcia-Orellana, J., Trezzi, G., Masqué, P., Stieglitz, T. C., Bokuniewicz, H., . . . Berdalet, E. (2017). Using the radium quartet to quantify submarine groundwater discharge and pore water exchange. *Geochimica et Cosmochimica Acta*, *196*, 58–73. https://doi.org/10.1016/j.gca.2016.09.016

Ryther, J. H., & Dunstan, W. M. (1971). Nitrogen, phosphorus, and eutrophication in the coastal marine environment. *Science*, *171*(3975), 1008–1013.

Santos, I. R., Burnett, W. C., Chanton, J., Dimova, N., & Peterson, R. N. (2009a). Land or ocean?: Assessing the driving forces of submarine groundwater discharge at a coastal site in the Gulf of Mexico. *Journal of Geophysical Research: Oceans*, *114*, C04012. https://doi.org/10.1029/2008JC005038

Santos, I. R., Burnett, W. C., Dittmar, T., Suryaputra, I. G., & Chanton, J. (2009b). Tidal pumping drives nutrient and dissolved organic matter dynamics in a Gulf of Mexico subterranean estuary. *Geochimica et Cosmochimica Acta*, *73*(5), 1325–1339.

Santos, I. R., Cook, P. L. M., Rogers, L., de Weys, J., & Eyre, B. D. (2012a). The ''salt wedge pump'': Convection-driven pore-water exchange as a source of dissolved organic and inorganic carbon and nitrogen to an estuary. *Limnology and Oceanography*, *57*(5), 1415–1426.

Santos, I. R., Eyre, B. D., & Huettel, M. (2012b). The driving forces of pore water and groundwater flow in permeable coastal sediments: A review. *Estuarine, Coastal and Shelf Science*, *98*(0), 1–15. https://doi.org/10.1016/j.ecss.2011.10.024

Sawyer, A. H., David, C. H., & Famiglietti, J. S. (2016). Continental patterns of submarine groundwater discharge reveal coastal vulnerabilities. *Science*, *353*(6300), 705–707.

Shaban, A., Khawlie, M., Abdallah, C., & Faour, G. (2005). Geologic controls of submarine groundwater discharge: Application of remote sensing to north Lebanon. *Environmental Geology*, *47*(4), 512–522.

Shang, S., Li, L., Sun, F., Wu, J., Hu, C., Chen, D., . . . Shang, S. (2008). Changes of temperature and bio-optical properties in the South China Sea in response to Typhoon Lingling, 2001. *Geophysical Research Letters*, *35*, L10602. https://doi.org/10.1029/2008GL033502

Siswanto, E., Ishizaka, J., Yokouchi, K., Tanaka, K., & Tan, C. K. (2007). Estimation of interannual and interdecadal variations of typhoon-induced primary production: A case study for the outer shelf of the East China Sea. *Geophysical Research Letters*, *34*, L03604. https://doi.org/10.1029/2006GL028368

Son, S., Platt, T., Bouman, H., Lee, D., & Sathyendranath, S. (2006). Satellite observation of chlorophyll and nutrients increase induced by Typhoon Megi in the Japan/East Sea. *Geophysical Research Letters*, *33*, L05607. https://doi.org/10.1029/2005GL025065

Song, X., Lai, Z., Ji, R., Chen, C., Zhang, J., Huang, L., . . . Zhu, X. (2012). Summertime primary production in northwest South China Sea: Interaction of coastal eddy, upwelling and biological processes. *Continental Shelf Research*, *48*, 110–121.

Stukel, M. R., Asher, E., Couto, N., Schofield, O., Strebel, S., Tortell, P., & Ducklow, H. W. (2015). The imbalance of new and export production in the Western Antarctic Peninsula, a potentially ''leaky'' ecosystem. *Global Biogeochemical Cycles*, *29*, 1400–1420. https://doi.org/10.1002/2015GB005211

Su, J., Wang, J., Pohlmann, T., & Xu, D. (2011). The influence of meteorological variation on the upwelling system off eastern Hainan during summer 2007–2008. *Ocean Dynamics*, *61*(6), 717–730. https://doi.org/10.1007/s10236-011-0404-9

Su, J., Xu, M., Pohlmann, T., Xu, D., & Wang, D. (2013). A western boundary upwelling system response to recent climate variation (1960–2006). *Continental Shelf Research*, *57*, 3–9.

Su, N., Du, J. Z., Moore, W. S., Liu, S. M., & Zhang, J. (2011). An examination of groundwater discharge and the associated nutrient fluxes into the estuaries of eastern Hainan Island, China using ^{226}Ra. *The Science of the Total Environment*, *409*(19), 3909–3918. https://doi.org/10.1016/J.Scitotenv.2011.06.017

Swarzenski, P. W., Reich, C. D., Spechler, R. M., Kindinger, J. L., & Moore, W. S. (2001). Using multiple geochemical tracers to characterize the hydrogeology of the submarine spring off Crescent Beach, Florida. *Chemical Geology*, *179*(1–4), 187–202.

Swarzenski, P. W., Simonds, F. W., Paulson, A. J., Kruse, S., & Reich, C. (2007). Geochemical and geophysical examination of submarine groundwater discharge and associated nutrient loading estimates into Lynch Cove, Hood Canal, WA. *Environmental Science & Technology*, *41*(20), 7022–7029. https://doi.org/10.1021/Es070881a

Talbot, J. M., Kroeger, K. D., Rago, A., Allen, M. C., & Charette, M. A. (2003). Nitrogen flux and speciation through the subterranean estuary of Waquoit Bay, Massachusetts. *Biological Bulletin*, *205*(2), 244–245.

Taniguchi, M., Burnett, W. C., Smith, C. F., Paulsen, R. J., O'rourke, D., Krupa, S. L., & Christoff, J. L. (2003). Spatial and temporal distributions of submarine groundwater discharge rates obtained from various types of seepage meters at a site in the Northeastern Gulf of Mexico. *Biogeochemistry*, *66*(1), 35–53.

Taniguchi, M., Ishitobi, T., Chen, J. Y., Onodera, S. I., Miyaoka, K., Burnett, W. C., Peterson, R., . . . Fukushima, Y. (2008). Submarine groundwater discharge from the Yellow River Delta to the Bohai Sea, China. *Journal of Geophysical Research: Oceans*, *113*, C06025. https://doi.org/10.1029/2007JC004498

Taniguchi, M., Ishitobi, T., & Shimada, J. (2006). Dynamics of submarine groundwater discharge and freshwater-seawater interface. *Journal of Geophysical Research: Oceans*, *111*, C01008. https://doi.org/10.1029/2005JC002924

Taniguchi, M., & Iwakawa, H. (2004). Submarine groundwater discharge in Osaka Bay, Japan. *Limnology*, *5*(1), 25–32. https://doi.org/10.1007/s10201-003-0112-3

Valiela, I., Foreman, K., LaMontagne, M., Hersh, D., Costa, J., Peckol, P., . . . Lajtha, K. (1992). Couplings of watersheds and coastal waters: Sources and consequences of nutrient enrichment in Waquoit Bay, Massachusetts. *Estuaries*, *15*(4), 443–457.

Valiela, I., Teal, J. M., Volkmann, S., Shafer, D., & Carpenter, E. J. (1978). Nutrient and particulate fluxes in a salt-marsh ecosystem: Tidal exchanges and inputs by precipitation and groundwater. *Limnology and Oceanography*, *23*(4), 798–812.

Van Der Loeff, M. R. (1981). Wave effects on sediment water exchange in a submerged sand bed. *Netherlands Journal of Sea Research*, *15*(1), 100–112.

Wang, D., Wang, H., Li, M., Liu, G., & Wu, X. (2013). Role of Ekman transport versus Ekman pumping in driving summer upwelling in the South China Sea. *Journal of Ocean University of China*, *12*(3), 355–365.

Wang, G., Jing, W., Wang, S., Xu, Y., Wang, Z., Zhang, Z., . . . Dai, M. (2014). Coastal acidification induced by tidal-driven submarine groundwater discharge in a coastal coral reef system. *Environmental Science & Technology*, *48*(22), 13069–13075. https://doi.org/10.1021/es5026867

Wang, S. H., Hsu, N. C., Tsay, S. C., Lin, N. H., Sayer, A. M., Huang, S. J., & Lau, W. K. (2012). Can Asian dust trigger phytoplankton blooms in the oligotrophic northern South China Sea? *Geophysical Research Letters*, *39*, L05811, https://doi.org/10.1029/2011GL050415

Wang, X., & Du, J. (2016). Submarine groundwater discharge into typical tropical lagoons: A case study in eastern Hainan Island, China. *Geochemistry, Geophysics, Geosystems*, *17*, 4366–4382. https://doi.org/10.1002/2016GC006502

Wang, X., Li, H., Jiao, J. J., Barry, D. A., Li, L., Luo, X., . . . Jiang, X. (2015b). Submarine fresh groundwater discharge into Laizhou Bay comparable to the Yellow River flux, *Scientific Reports*, *5*, 8814.

Wong, G. T. F., Ku, T. L., Mulholland, M., Tseng, C. M., & Wang, D. P. (2007). The South East Asian time-series study (SEATS) and the biogeochemistry of the South China Sea: An overview. *Deep Sea Research Part II: Topical Studies in Oceanography*, *54*(14–15), 1434–1447. https://doi.org/10.1016/j.dsr2.2007.05.012

Wong, G. T. F., Pan, X., Li, K.-Y., Shiah, F.-K., Ho, T.-Y., & Guo, X. (2015). Hydrography and Nutrient dynamics in the northern South China Sea Shelf-sea (NoSoCS). *Deep Sea Research Part II: Topical Studies in Oceanography*, *117*, 23–40.

Wu, J., Chung, S.-W., Wen, L.-S., Liu, K.-K., Chen, Y-L. L., Chen, H.-Y., & Karl, D. M. (2003). Dissolved inorganic phosphorus, dissolved iron, and Trichodesmium in the oligotrophic South China Sea. *Global Biogeochemistry Cycles*, *17*(1), 1008. https://doi.org/10.1029/2002GB001924

Younger, P. L. (1996). Submarine groundwater discharge. *Nature*, *382*(6587), 121–122.

Zhang, J., Wang, D. R., Jennerjahn, T., & Dsikowitzky, L. (2013). Land–sea interactions at the east coast of Hainan Island, South China Sea: A synthesis. *Continental Shelf Research*, *57*, 132–142.

Zhang, R., Chen, M., Yang, Q., Lin, Y., Mao, H., Qiu, Y., . . . Cao, J. (2015). Physical-biological coupling of N_2 fixation in the northwestern South China Sea coastal upwelling during summer. *Limnology and Oceanography*, *60*(4), 1411–1425. https://doi.org/10.1002/lno.10111

Zhou, Z.-G. (2005). Characteristics and utilization of groundwater resources in Hainan Island [J]. *Water Resources Protection*, *3*, 016.